Hbp1 regulates the timing of neuronal differentiation during cortical development by controlling cell cycle progression

Naoki Watanabe[1,2,3], Ryoichiro Kageyama[1,2,3,4,5] and Toshiyuki Ohtsuka[1,2,3,4,*]

ABSTRACT

In the developing mammalian brain, neural stem cells (NSCs) initially expand the progenitor pool by symmetric divisions. NSCs then shift from symmetric to asymmetric division and commence neurogenesis. Although the precise mechanisms regulating the developmental timing of this transition have not been fully elucidated, gradual elongation in the length of the cell cycle and coinciding accumulation of determinants that promote neuronal differentiation might function as a biological clock that regulates the onset of asymmetric division and neurogenesis. We conducted gene expression profiling of embryonic NSCs in the cortical regions and found that expression of high mobility group box transcription factor 1 (*Hbp1*) was upregulated during neurogenic stages. Induced conditional knockout mice of *Hbp1*, generated by crossing with *Nestin-CreER*^{T2} mice, exhibited a remarkable dilatation of the telencephalic vesicles with a tangentially expanded ventricular zone and a thinner cortical plate containing reduced numbers of neurons. In these *Hbp1*-deficient mouse embryos, neural stem/ progenitor cells continued to divide with a shorter cell cycle length. Moreover, downstream target genes of the Wnt signaling, such as cyclin D1 (*Ccnd1*) and *c-jun* (*Jun*), were upregulated in the germinal zone of the cortical regions. These results indicate that Hbp1 plays a crucial role in regulating the timing of cortical neurogenesis by elongating the cell cycle and that it is essential for normal cortical development.

KEY WORDS: Hbp1, Brain morphology, Cell cycle, Cortical development, Neural stem cells, Neuronal differentiation, Mouse

INTRODUCTION

During mammalian cortical development, neural stem cells (NSCs) gradually alter their characteristics and generate a variety of cell types, which establishes the functional complexity of the brain (Temple, 2001). In early developmental stages, a sheet of NSCs vigorously expands through repeated symmetric divisions, and the neural tube distends like a balloon, with a thin wall composed of short neuroepithelial cells. After expanding the progenitor pool for several cycles, NSCs in the cortical regions begin to produce neurons by converting from symmetric to asymmetric division, which initiates neurogenesis (Takahashi et al., 1995, 1999). The timing of this transition is crucial for determining the overall

number of NSCs and the size of ventricles, which largely determines the eventual size and morphology of the brain. However, the precise mechanisms that regulate the switch from symmetric to asymmetric division and the onset of neurogenesis have not been fully elucidated.

It has been reported that the length of the G1 phase of the cell cycle (T_{G1}) in neural stem/progenitor cells gradually rises over the course of cortical development. This elongation of T_{G1} is accompanied by downregulation of cyclin E (Ccne1 – Mouse Genome Informatics) and p21 (Cdkn1a – Mouse Genome Informatics), along with upregulation of p27 (Cdkn1b – Mouse Genome Informatics), cdk2 and cyclin B (Delalle et al., 1999; Caviness et al., 2003). Moreover, the forced reduction of T_{G1} by manipulation of cyclin D1 led to an expansion of neural progenitor cells in the developing and adult brain (Lange et al., 2009; Pilaz et al., 2009; Artegiani et al., 2011). One proposed mechanism for the transition from symmetric proliferative to asymmetric neurogenic division is that an elongation of T_{G1} allows fate determinants that promote neuronal differentiation to accumulate during the G1 phase and exert their neurogenic functions (Calegari and Huttner, 2003; Calegari et al., 2005; Götz and Huttner, 2005; Dehay and Kennedy, 2007).

To identify temporal alterations in the transcriptional properties of embryonic NSCs, we previously carried out DNA microarray-based gene expression profiling of embryonic NSCs prepared from the cortical regions at different developmental stages by using *pHes1-d2EGFP* transgenic mice, which express enhanced green fluorescent protein (*EGFP*) in NSCs (Ohtsuka et al., 2006, 2011). Among a variety of genes that were differentially expressed during the course of development, we hypothesized that high mobility group box transcription factor 1 (*Hbp1*) might be an important regulator of neurogenesis, given that it was upregulated during neurogenic stages around embryonic day 13.5 (E13.5) through embryonic day 15.5 (E15.5). Previous studies demonstrated that Hbp1 acts as a transcriptional repressor that functions as a cell cycle inhibitor by repressing downstream targets of the Wnt signaling and cell cycle-related genes, cyclin D1 (*Ccnd1*), *c-jun* (*Jun*), N-myc (*Mycn*) and *p21* (*Cdkn1a*) (Gartel et al., 1998; Sampson et al., 2001; Kim et al., 2006; Elfert et al., 2013; Yan et al., 2014).

Here, we analyzed the molecular function of Hbp1 in neuronal differentiation during cortical development. We found that Hbp1 controls the length of the cell cycle in neural stem/progenitor cells by modulating the expression levels of cyclin D1, thereby regulating the timing of neuronal differentiation during early cortical development.

RESULTS

Hbp1 is expressed in the germinal zone during cortical neurogenesis

By evaluating our gene expression profiling data for embryonic NSCs in the developing cortex (Ohtsuka et al., 2011), we selected

[1]Institute for Virus Research, Kyoto University, Shogoin-Kawahara, Sakyo-ku, Kyoto 606-8507, Japan. [2]Japan Science and Technology Agency, Core Research for Evolutional Science and Technology (CREST), 4-1-8 Honcho, Kawaguchi, Saitama 332-0012, Japan. [3]Graduate School of Medicine, Kyoto University, Kyoto 606-8501, Japan. [4]Graduate School of Biostudies, Kyoto University, Kyoto 606-8501, Japan. [5]World Premier International Research Initiative-Institute for Integrated Cell-Material Sciences (WPI-iCeMS), Kyoto University, Kyoto 606-8501, Japan.

*Author for correspondence (tohtsuka@virus.kyoto-u.ac.jp)

candidate genes expected to be involved in the regulation of neuronal differentiation based on their upregulation during the neurogenic period. Among these genes, we observed that *Hbp1* was prominently expressed in the germinal zone that comprises the ventricular zone (VZ) and subventricular zone (SVZ) in the developing telencephalon (Fig. 1A). The expression pattern of *Hbp1* was characterized by a lateral high-dorsal low gradient at E11.5 corresponding to the propagation of neurogenesis, similar to the expression pattern of *Neurog2*, a proneural (neurogenic) basic helix-loop-helix (bHLH) gene (Fig. 1B). As it was difficult to accurately estimate alterations in *Hbp1* expression levels over the course of development by *in situ* hybridization, we performed real-time RT-PCR using total RNAs prepared from NSCs in the cortical regions of *pHes1-d2EGFP* transgenic mice at different embryonic
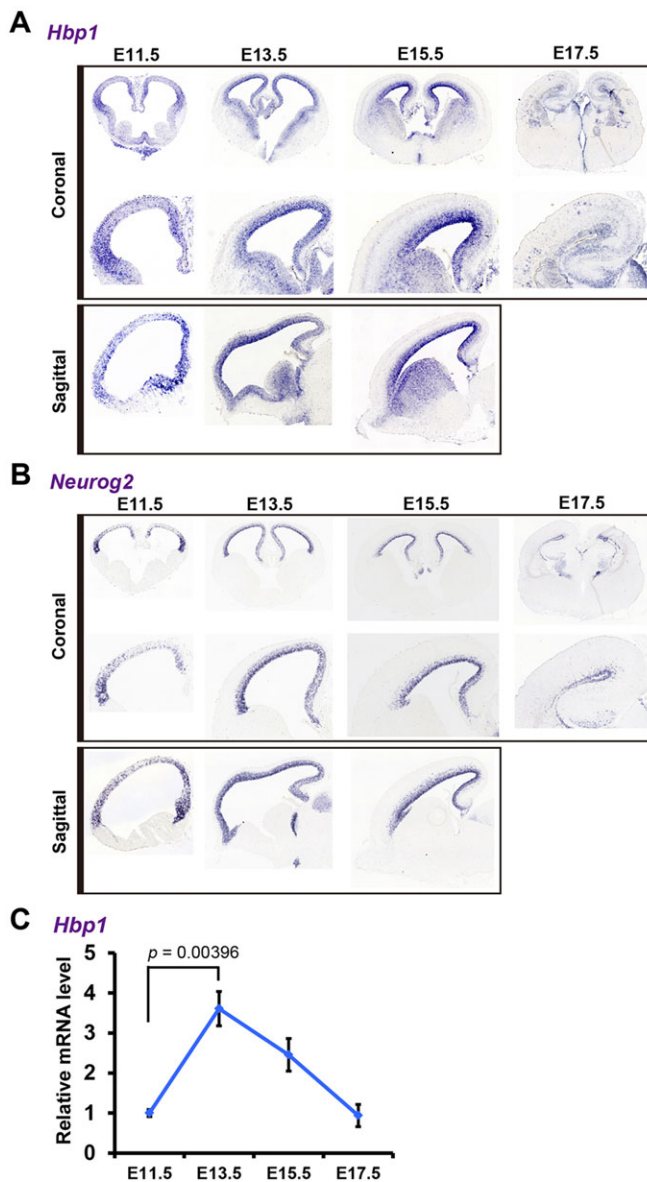

Fig. 1. Temporal and spatial expression patterns of *Hbp1* in the developing brain. (A,B) *In situ* hybridization for *Hbp1* (A) or *Neurog2* (B) was performed on coronal and sagittal (rostral, left; caudal, right) sections of the telencephalon of mouse embryos at various developmental stages. (C) Real-time RT-PCR for *Hbp1* using total RNAs prepared from NSCs in the cortical regions of *d2EGFP* transgenic mice. *β-actin* was used as internal control, and the values were normalized to that of the E11.5 sample. *n*=3, error bars: s.e.m.

stages and confirmed the temporal dynamics of *Hbp1* expression indicated by microarray analysis (Fig. 1C).

Overexpression of Hbp1 suppresses cell proliferation, but inhibits terminal neuronal differentiation

We conducted overexpression experiments by *in utero* electroporation. *Hbp1* expression vectors (*pEF-Hbp1*) and control vectors (*pEF-EGFP*) were co-introduced into ventricular cells in the cortical regions of E13.5 mouse embryos, and the fates of transfected cells were subsequently examined at E14.5 and E16.5. As shown in our previous paper (Ohtsuka et al., 2011), cells transfected with *pEF-Hbp1* mainly remained in the SVZ and the intermediate zone (IZ) at E16.5. Noticeably, a majority of transfected cells differentiated into neurons positive for neuronal markers, such as Tuj1 (Tubb3 – Mouse Genome Informatics) and Map2. In addition, they were negative for Ki67 (Mki67 – Mouse Genome Informatics), a marker of proliferating cells, or phospho-histone H3 (pH3), a marker of dividing cells in the M phase; moreover, they stagnated in the IZ and failed to migrate into the cortical plate (CP) (Fig. 2A; supplementary material Fig. S1A-D), indicating that neuronal migration was inhibited. The proportions of transfected cells positive for Pax6, a specific marker of NSCs during this period of development, and Tbr2 (Eomes – Mouse Genome Informatics), a marker of intermediate progenitor cells (IPs), were significantly lower than in the control at E16.5. Transfected cells that incorporated BrdU administered 4 h after *in utero* electroporation at E13.5 exited the VZ earlier than control cells at E15.5. However, the majority of cells still remained in the IZ at E16.5 (supplementary material Fig. S1E,F), suggesting that overexpression of Hbp1 promoted initial neuronal differentiation but impaired terminal neuronal differentiation and migration.

Next, we evaluated the rate of cell proliferation by administering the thymidine analog EdU intraperitoneally to the pregnant mice 30 min before sacrifice at E14.5 to mark cells in the S phase. In cells transfected with *pEF-Hbp1*, EdU incorporation was suppressed compared with control (Fig. 2B), indicating that overexpression of Hbp1 caused an attenuation of cell proliferation or premature cell cycle exit. We then carried out a calculation of cell cycle kinetics by BrdU/EdU double-labeling protocol [modified from a previously described IdU/BrdU double-labeling method (Martynoga et al., 2005; Mairet-Coello et al., 2012)] and estimated the cell cycle length. Cells transfected with *pEF-Hbp1* showed a slightly longer cell cycle length compared with control (Fig. 8F; supplementary material Table S3); however, the effect on the cell cycle was minimal in comparison with *Hbp1* knockdown or *Hbp1*-deficient cells.

Co-expression of Rb1 de-represses terminal neuronal differentiation and migration

Hbp1 has been shown to be a target of retinoblastoma 1 (Rb1) and p130, also known as Rbl2 (Tevosian et al., 1997). Shih et al. reported that muscle cell differentiation was blocked when Hbp1 was overexpressed in C2C12 cells without interfering with cell cycle exit, and the expression of MyoD (Myod1 – Mouse Genome Informatics) and myogenin (Myog), but not of Myf5, was inhibited in Hbp1-expressing cells; however, full differentiation occurred when Rb1 was co-expressed with Hbp1 and the ratio of Rb1/Hbp1 was elevated, suggesting that the relative ratio of Rb1 to Hbp1 is important as a determinant of whether cell cycle exit or full differentiation occurs (Shih et al., 1998). Thus, we introduced a mixture of *pEF-Hbp1* and *pCAGGS-HA-human Rb1* (*hRb1*) vectors at ratios of 3:1 or 1:3 by *in utero* electroporation, and found that transfected cells were released from the stagnation and significantly more transfected cells reached the CP when Hbp1 and Rb1 were co-expressed (Fig. 2C,D).

Next, we examined the expression levels of proneural bHLH genes by *in situ* hybridization 24 h after *in utero* electroporation. We found that *Neurod1* expression was downregulated in the regions transfected with *pEF-Hbp1* (Fig. 2E), and the repression was rescued to some extent by co-expression of Rb1, whereas expression of *Neurog2* was not significantly affected. Taken together, these results supported findings from a previous study of muscle cell differentiation (Shih et al., 1998) and also suggested that overexpression of Hbp1 promoted cell cycle exit but impaired terminal neuronal differentiation required for full migration due to the low Rb1/Hbp1 ratio. Conversely, a higher Rb1/Hbp1 ratio

obtained by co-expressing Rb1 promoted terminal differentiation and neuronal migration.

Knockdown of *Hbp1* inhibits neuronal differentiation and activates cell cycle progression

Next, we carried out knockdown experiments using expression vectors of shRNA targeting *Hbp1* (*shHbp1*), in addition to scrambled shRNA control vectors (*scrambled*) (supplementary material Fig. S2A,B). When we introduced *shHbp1* into ventricular cells together with *pEF-EGFP* by *in utero* electroporation at E13.5, most cells transfected with *shHbp1* remained in the VZ/SVZ/IZ,
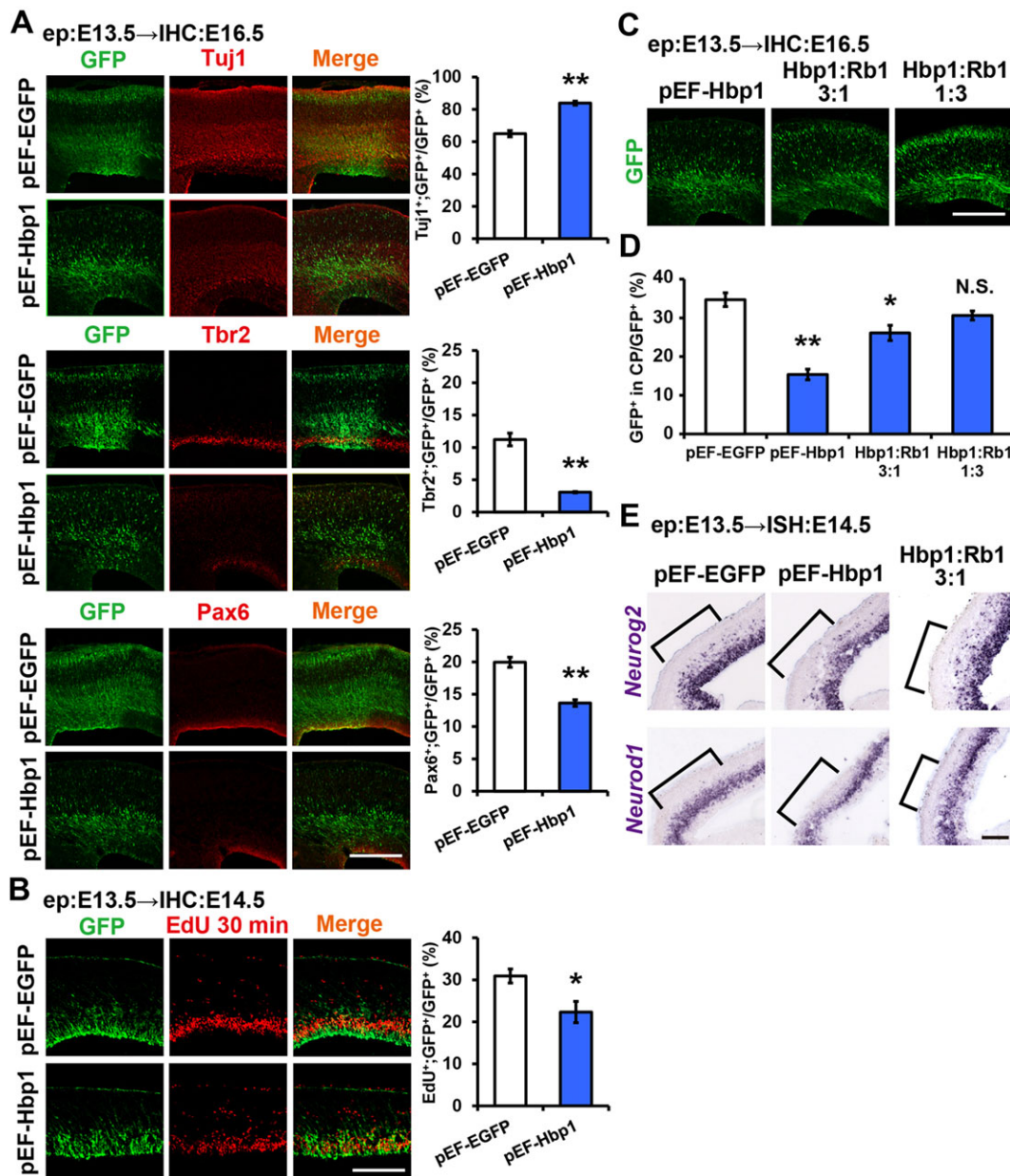

Fig. 2. Inhibition of terminal neuronal differentiation and migration by overexpression of Hbp1. *In utero* electroporation (ep) was performed with control vectors (*pEF-EGFP*) alone or with a combination of *Hbp1* expression vectors (*pEF-Hbp1*) at E13.5. The fates of transfected cells were analyzed at E14.5 (B) or E16.5 (A,C) by immunohistochemistry (IHC). (A) Coronal sections of dorsolateral telencephalon were double-stained using anti-GFP (green) and anti-Tuj1/Tbr2/Pax6 (red) antibodies. (B) EdU was administered intraperitoneally to pregnant mice 30 min before sacrifice, and incorporated EdU (red) was detected by a fluorogenic click reaction. (C) *pCAGGS-HA-hRb1* vectors were co-transfected with *pEF-Hbp1* at ratios of 3:1 or 1:3 by *in utero* electroporation at E13.5, and the fates of transfected cells were analyzed at E16.5. (D) The proportions of transfected cells that migrated into the cortical plate are shown in bar graphs. (E) *In situ* hybridization for neurogenic bHLH genes such as *Neurog2* and *Neurod1* was performed on coronal brain sections 24 h after *in utero* electroporation at E14.5. Brackets indicate regions transfected with expression vectors. *n*=3, error bars: s.e.m.; *$P<0.05$, **$P<0.01$; Student's *t*-test; N.S., not significant. Scale bars: 200 μm.

with only a few cells observed in the CP at E16.5 (supplementary material Fig. S2C). However, neuronal differentiation occurred later and most transfected cells in the IZ were Tuj1 and Map2-positive and negative for Ki67 or pH3 (supplementary material Fig. S1A,C and Fig. S2C), although the number of pH3$^+$ cells increased in the VZ and SVZ in regions transfected with *shHbp1* (supplementary material Fig. S1C,D). Knockdown cells that incorporated BrdU administered 4 h after electroporation exhibited slower exits from the VZ than in the control at E15.5 (supplementary material Fig. S1E,F), indicating that *Hbp1* knockdown inhibited and delayed neuronal differentiation. Whereas most cells transfected with scrambled shRNA differentiated into Cux1$^+$ neurons (layer II-IV) and settled in the CP at E18.5, a majority of cells transfected with *shHbp1* still remained in the VZ/SVZ/IZ (supplementary material Fig. S2D). The number of Cux1$^+$ cells in the superficial layers of the CP decreased markedly in the regions transfected with *shHbp1*, whereas the number of Ctip2$^+$ cells (layer V) was comparable to the control.

To evaluate the specificity of the *Hbp1* knockdown, we performed rescue experiments by co-electroporation of *shHbp1* and *pEF-Hbp1* at ratios of 3:1, 1:1 or 1:3, and found that *pEF-Hbp1* rescued the phenotype of *Hbp1* knockdown (inhibition of neuronal differentiation and migration) at a 1:1 ratio (supplementary material Fig. S2E,F). However, the neuronal migration defect was observed again at a 1:3 ratio, similar to our observations in the case of Hbp1 overexpression.

We performed immunostaining with anti-phosphorylated vimentin (p-Vim) antibody but did not observe a significant increase in p-Vim$^+$ mitotic radial glial cells outside the VZ (supplementary material Fig. S1C,D). In addition, we found that cell death (as measured by cleaved-caspase 3$^+$ cells) was not enhanced by either overexpression or knockdown of Hbp1 at 3 days after electroporation (supplementary material Fig. S1G,H). Estimation of the cell cycle length revealed that *Hbp1* knockdown cells showed a considerably shorter cell cycle length compared with control (Fig. 8F; supplementary material Table S3), indicating that knockdown of *Hbp1* shortened the cell cycle length, in particular the duration of the G2-M-G1 phase, and activated cell cycle progression.

Deficiency of *Hbp1* in neural stem/progenitor cells impairs cortical morphogenesis

To analyze the function of Hbp1 over the course of brain development, we generated *Hbp1* induced conditional knockout (icKO) mice, in which tamoxifen-inducible Cre recombinase is expressed specifically in neural stem/progenitor cells in the embryonic brain (see supplementary materials and methods and Fig. S3A,B). We confirmed by real-time RT-PCR that expression of *Hbp1* in the telencephalon of *Hbp1* icKO mice was downregulated by E11.5 when tamoxifen was administered at E9.5 (supplementary material Fig. S3C).

The whole brain size of *Hbp1* icKO embryos was comparable to that of the negative controls (NC) but the telencephalic wall appeared to be thinner (Fig. 3A). The telencephalic vesicles of mutant embryos were remarkably dilated, although the ventricular dilatation was not prominent at E12.5 (Fig. 3A,B). The volume of the ventral telencephalon was severely diminished and the wall of the dorsal telencephalon was significantly thinner than that of the control after E14.5 (Fig. 3B). Notably, the ventricular surface area in the dorsolateral telencephalon (cortical region) was substantially enlarged; thus, the VZ appeared to be stretched in the tangential direction. The thickness of both the VZ (Pax6$^+$) and the neuronal

layer (Tuj1$^+$) were thinner than in the control. The midline and medial structures of the telencephalon, such as hippocampus and corpus callosum, were hypoplastic or missing at E18.5. The measurements of each structure are summarized in Fig. 3C (see supplementary materials and methods).

Hbp1-deficiency leads to delayed neuronal differentiation and tangential expansion of NSCs

Next, we investigated the dynamics of cortical development in the *Hbp1*-deficient mice. We determined the number of distinct cell types through immunolabeling with various cell- and layer-specific markers within a radial column of constant width (200 μm) in the cortical regions (Fig. 4A-C; supplementary material Fig. S4A,B). At E12.5, the thickness of the VZ (Pax6$^+$ and Hes1$^+$) was similar to that in the control mice. Noticeably, the number of Tbr2$^+$ cells and early-born neurons (Tuj1$^+$ and Tbr1$^+$) was reduced in the icKO mice at E12.5, indicating that the onset of neurogenesis was delayed. Instead, the NSC population was still expanding by symmetric divisions, thus leading to the tangential extension of the VZ and ventricular dilatation that became prominent after E14.5. We determined the number of Pax6$^+$ NSCs throughout the cortical regions in multiple coronal sections at constant intervals along the antero-posterior axis of lateral ventricle. Through this method, we estimated and compared the total number of NSCs in the hemisphere of control and mutant brains, and found that the total number of NSCs was increased in the icKO at E14.5 (Fig. 3C).

As the generation of Tbr2$^+$ IPs and neurons commences after the transition from symmetric to asymmetric division mode of NSCs (Sessa et al., 2008), these results suggested that the *Hbp1*-deficiency delayed this transition and the onset of neurogenesis. Thus, we analyzed the fates of cells after cell divisions by administering EdU 12 h before sacrifice (Fig. 5A). A majority of cells that incorporated EdU remained Pax6$^+$ NSCs in the cortical regions of icKO embryos at E12.5, whereas the number of EdU$^+$ cells that differentiated into Tbr2$^+$ IPs was much higher in the control (Fig. 5B). Given the significantly higher frequency of cell divisions in Pax6$^+$ cells than in Tbr2$^+$ cells, as demonstrated by pH3 staining (Fig. 5C), these results indicated that the symmetric proliferative divisions of Pax6$^+$ NSCs were maintained in the icKO at a population level, although it was not revealed at a single-cell level, whereas many NSCs had shifted to asymmetric neurogenic division in the control at E12.5. Estimation of the proportions of Ki67$^+$;EdU$^+$/EdU$^+$ (cell cycle re-entry) and Ki67$^-$; EdU$^+$/EdU$^+$ (cell cycle exit) also indicated that more cells re-entered the cell cycle in the icKO, whereas more cells exited the cell cycle in the control at E12.5 and E14.5 (Fig. 5D).

Cortical neurons are reduced in number proportionately throughout all layers

Immunostaining with anti-Pax6 and anti-Hes1 antibodies revealed that the thickness of the VZ was reduced in the icKO mice compared with control at E14.5 and thereafter (Fig. 4A-C; supplementary material Fig. S4A,B). Intriguingly, the number of Tbr2$^+$ cells remarkably increased in the mutant cortex by E14.5 (Fig. 4A-C), and EdU incorporation experiments revealed that those Tbr2$^+$ cells were highly proliferative at E14.5 (Fig. 5A,B); however, Tbr2$^+$ IPs rapidly reduced in number between E14.5 and E16.5. These results indicated a drastic thinning of the germinal zone composed of NSCs and IPs at later stages. We found that cell death was enhanced in Pax6$^+$, Tbr2$^+$ and Tuj1$^+$ populations in the icKO (supplementary material Fig. S5A,B), suggesting that the cell death somewhat

masked the expansion of NSCs through continued symmetric divisions and caused the reduction of neural stem/progenitor cells at later stages. Enhanced cell death was also observed in the ventral telencephalon (supplementary material Fig. S5C,D). However, in the cortical regions, no significant difference was observed in the number of GABA (γ-aminobutyric acid)-positive GABAergic interneurons, which are generated in the ventral telencephalon (data not shown).

The thickness of the cortical neuronal layers was reduced in the icKO throughout embryonic stages, as estimated by Tuj1 expression in the IZ/CP and expression of NeuN (Rbfox3), a neuronal marker,

in the CP (supplementary material Fig. S4A,B). We counted the number of cells positive for each marker and then normalized to the number of all DAPI$^+$ nuclei. We found that the subsets of layer-specific neurons were proportionately reduced in the icKO at all stages analyzed (Fig. 4C). It is likely that the significant cell death and rapid depletion of the neural stem/progenitor cell pool contributed to the reduced thickness of cortical layers.

In situ hybridization and real-time RT-PCR revealed that the expression levels of *Neurog2* and *Neurod1* were prominently upregulated around E14.5-16.5 in the mutant cortex (Fig. 6A,B), whereas expression of *Ascl1* (achaete-scute complex homolog 1) was
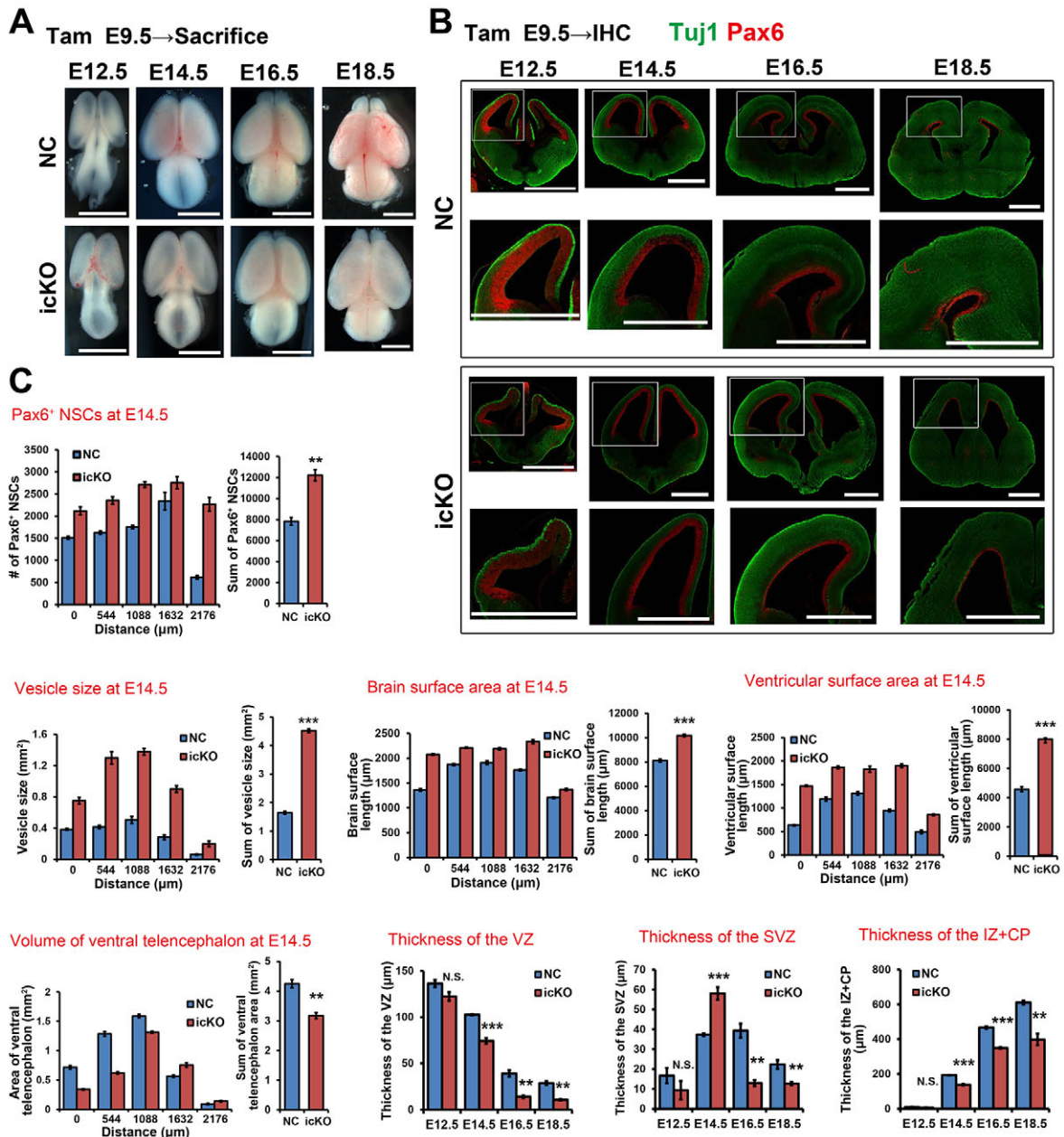

Fig. 3. Impaired cortical morphogenesis in *Hbp1* icKO mice. Tamoxifen (Tam) was administered at E9.5 and embryos were sacrificed at the indicated stages. (A) Images of whole brains at different embryonic stages comparing the gross shape and size of the brains (dorsal view) of negative control (NC) and *Hbp1* icKO mice. (B) Immunohistochemistry on coronal sections using anti-Tuj1 (green) and anti-Pax6 (red) antibodies. The boxed areas are shown in higher magnification in the bottom panels. (C) The numbers of Pax6$^+$ NSCs in hemispheres were estimated and compared between the control and the icKO mice at E14.5; the vesicle size of lateral ventricle, the length of brain surface and ventricular surface in cortical regions, the area of ventral telencephalon and the thickness of each cortical layer (VZ, SVZ and IZ+CP) were measured and compared between the control and the icKO mice at E14.5. *n*=3, error bars: s.e.m.; **$P<0.01$, ***$P<0.001$; Student's *t*-test; N.S., not significant. Scale bars: 2 mm in A; 1 mm in B.
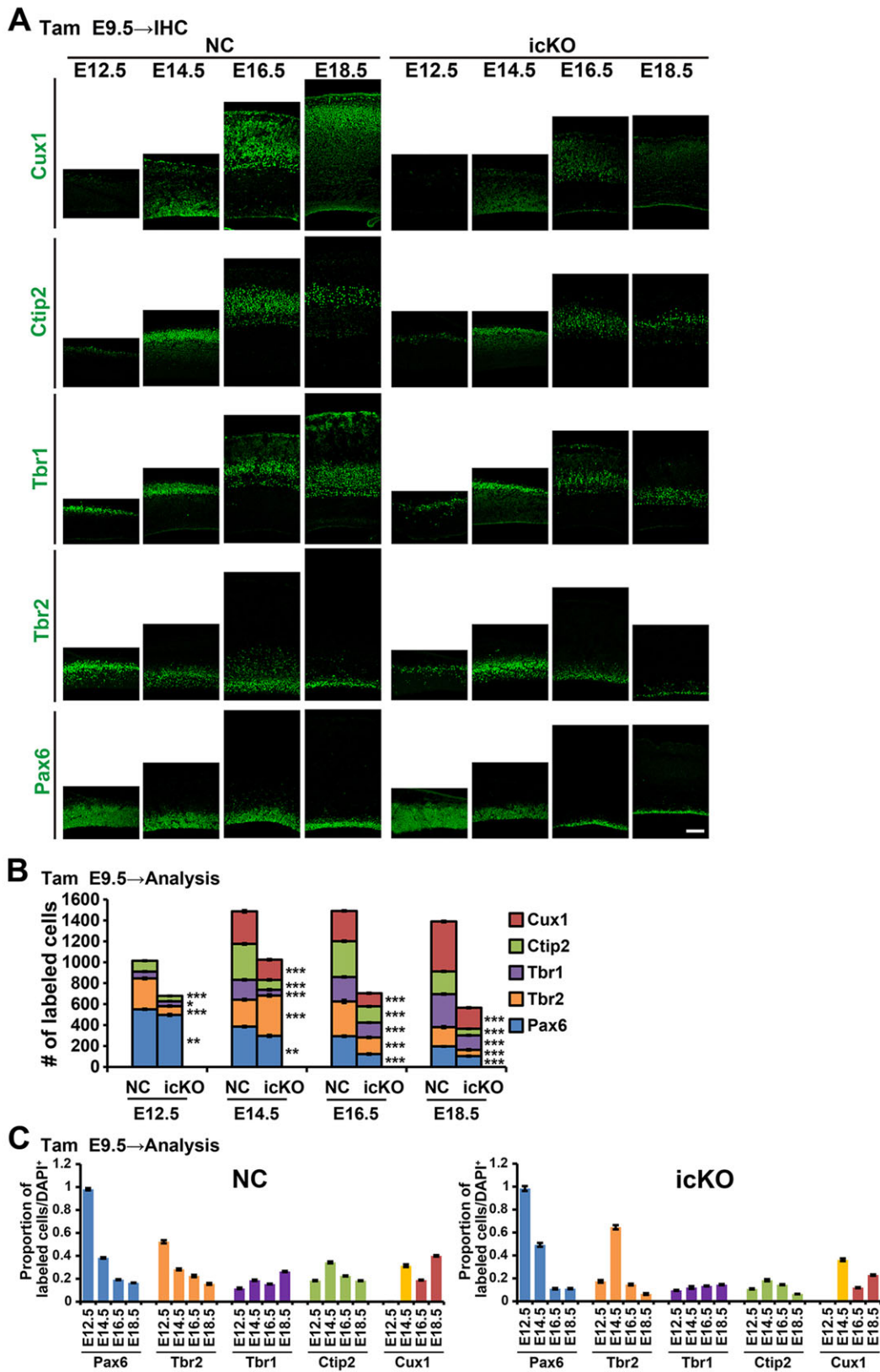
Fig. 4. Perturbed cortical neurogenesis in *Hbp1*-deficient mice. (A) Immunohistochemistry on coronal sections of the cortical regions of negative control (NC) and *Hbp1* icKO mice at different developmental stages with markers specific to each cortical layer (Cux1 for layer II-IV, Ctip2 for layer V and Tbr1 for layer VI), Tbr2, a marker for IPs, and Pax6, a marker for NSCs. (B) The number of cells immunoreactive for each antibody was counted within a radial column of 200 μm width in the middle part of dorsolateral telencephalon. (C) The proportions of cells positive for each marker of all DAPI$^+$ cells within the radial column. Cux1$^+$ cells in the VZ/SVZ/IZ are shown in yellow bars and those in the CP are shown in red. n=3, error bars: s.e.m.; *P<0.05, **P<0.01, ***P<0.001; Student's t-test. Scale bar: 100 μm.
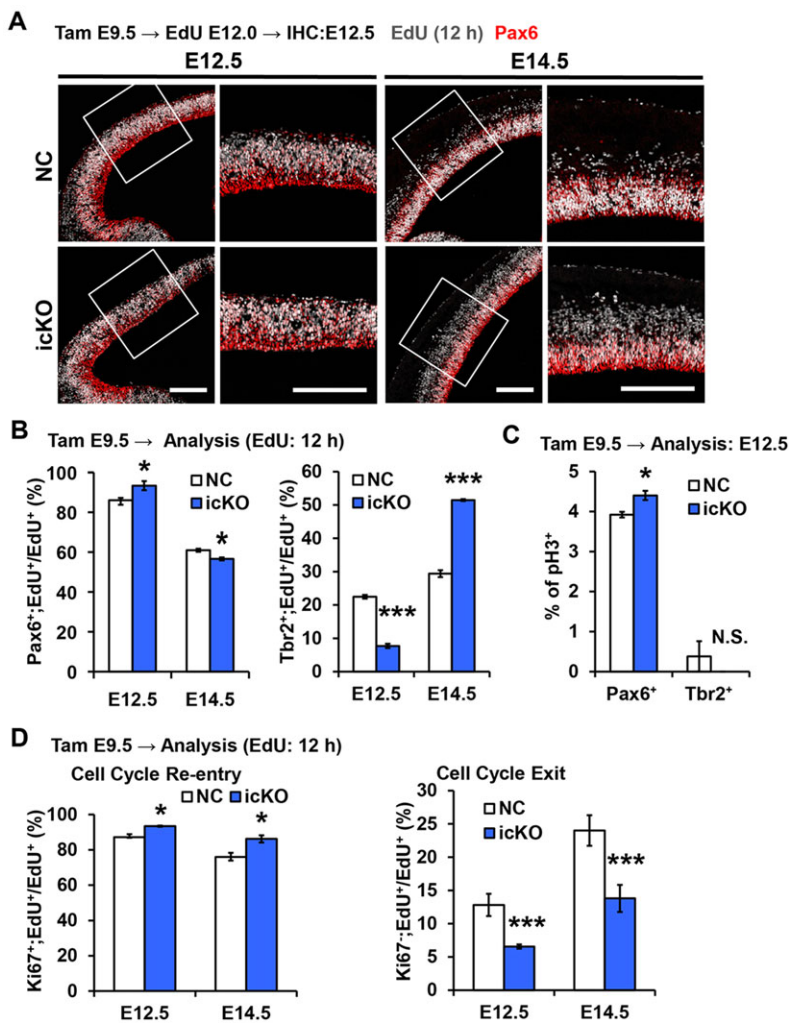
Fig. 5. Prolonged symmetric cell division and delayed neuronal differentiation. (A) EdU was administered intraperitoneally to pregnant mice 12 h before sacrifice, and the fate of cells that incorporated EdU were analyzed by immunolabeling, using anti-Pax6 and anti-Tbr2 antibodies. EdU$^+$ cells are shown in gray and Pax6$^+$ cells are shown in red. Boxed areas are shown in higher magnification on the right. (B) Graphs showing the proportions of Pax6$^+$ or Tbr2$^+$ cells of EdU-incorporated cells. (C) The proportions of pH3$^+$ cells of Pax6$^+$ or Tbr2$^+$ cells at E12.5. (D) The proportions of EdU/Ki67 double-positive (cell cycle re-entry) or EdU single-positive cells (cell cycle exit) of the total number of EdU$^+$ cells 12 h after administration of EdU. $n=3$, error bars: s.e.m.; *$P<0.05$, ***$P<0.001$; Student's t-test; N.S., not significant. Scale bars: 200 µm.

not significantly affected. We further assessed whether neurogenesis terminated earlier and gliogenesis began precociously in the icKO. Although aberrant generation of astrocytes (GFAP$^+$) or oligodendrocytes (Olig2$^+$) was not observed at either E16.5 or E18.5 (data not shown), the number of oligodendrocyte precursor cells (PDGFRα$^+$) decreased in the mutant cortex (supplementary material Fig. S4C,D), probably due to enhanced cell death and shrinking of the ventral telencephalon. It is possible that the sustained expression of neurogenic bHLH factors prevented precocious gliogenesis in the mutant brain (Sun et al., 2001). We also did not observe any significant increase of p-Vim$^+$ basal radial glial cells in the SVZ/OSVZ (outer subventricular zone) of mutant cortex at either E16.5 or E18.5 (supplementary material Fig. S4C,D).

Neural stem/progenitor cells are actively dividing in *Hbp1*-deficient mice

It was previously reported that Hbp1 is involved in regulation of the Wnt signaling by inhibiting the function of TCF4-β-catenin complex via physical blockade of TCF/LEF-mediated DNA binding, and functions as a growth suppressor by repressing downstream genes of the Wnt signaling and cell cycle-related genes (Tevosian et al., 1997; Gartel et al., 1998; Sampson et al., 2001; Shih et al., 2001; Kim et al., 2006; Elfert et al., 2013; Yan et al., 2014). We therefore assessed cell proliferation activity in neural stem/progenitor cells in the developing cortex. The number of cycling cells that incorporated EdU for 30 min before sacrifice, as well as proliferating cells (Ki67$^+$) and mitotic cells

(pH3$^+$), was significantly higher in the icKO at E14.5 (Fig. 7A,B). We then calculated the proportions of proliferating and mitotic Pax6$^+$ cells and Tbr2$^+$ cells separately, and determined that both cell types were more proliferative than in the control (Fig. 7C). The proportions of Ki67$^+$ cells that co-expressed Pax6 or Tbr2, and the proportions of Pax6$^+$ or Tbr2$^+$ cells that co-expressed Ki67, are shown in supplementary material Fig. S6.

Furthermore, we found that the cell cycle length was much shorter in neural stem/progenitor cells (Ki67$^+$) in the mutant cortex at each developmental stage (Fig. 7D; supplementary material Table S3). Intriguingly, the length of the overall cell cycle (T$_C$) was gradually elongated as development proceeded in both the control and the mutant cortex. The length of the S phase (T$_S$) was also shortened in the mutant cortex, although it was less prominent than the reduction in T$_C$ and comparatively constant during this period. These results indicate that the duration of the G2-M-G1 phase was significantly shortened in the *Hbp1* icKO mice. We then analyzed the cell cycle length separately in either Pax6$^+$ NSCs or Tbr2$^+$ IPs and found that both populations exhibited a shorter cell cycle (Fig. 7E,F; supplementary material Table S3).

Growth regulatory genes are upregulated in *Hbp1* knockdown and *Hbp1*-deficient cells

We next searched for genes that prospectively lay downstream of Hbp1. Immunohistochemistry and *in situ* hybridization revealed that cyclin D1 expression was remarkably upregulated in *Hbp1*
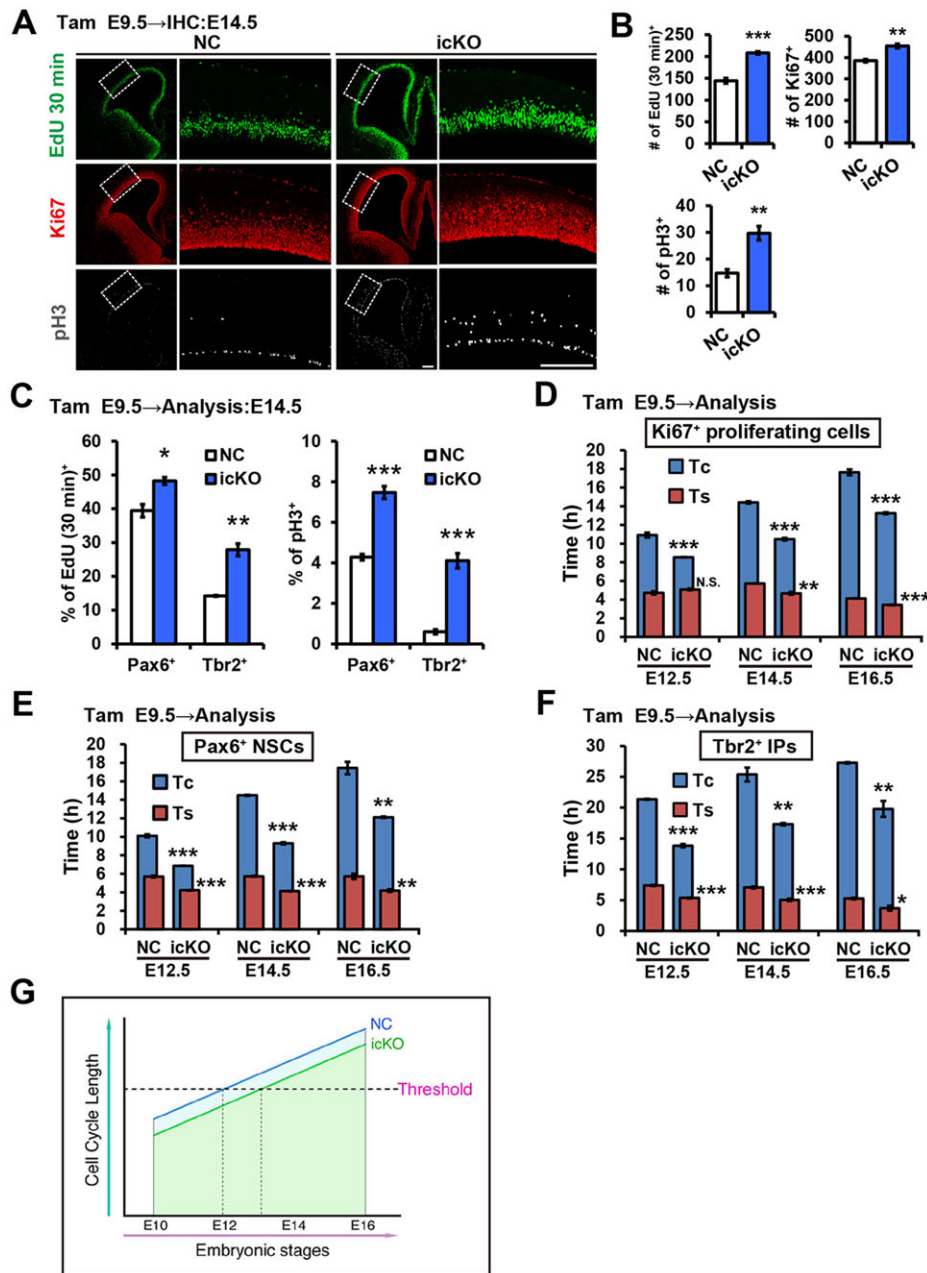
DEVELOPMENT

Fig. 6. Upregulated expression of neurogenic bHLH genes. (A) *In situ* hybridization (ISH) for neurogenic bHLH genes, such as *Neurog2*, *Ascl1* and *Neurod1*, on coronal brain sections of negative control (NC) and *Hbp1* icKO mice. Dashed lines indicate the ventricular surface. (B) Real-time RT-PCR showing the temporal expression patterns of *Neurog2*, *Ascl1* and *Neurod1*. *β-actin* was used as internal control, and the values were normalized to that of the E12.5 NC sample. *n*=3, error bars: s.e.m.; *$P<0.05$, **$P<0.01$; Student's *t*-test; N.S., not significant. Scale bar: 100 μm.

knockdown cells (Fig. 8A,B; supplementary material Fig. S7A). In addition, we estimated cyclin D1 expression levels and found that the proportion of cyclin D1-expressing GFP⁺ cells was not significantly changed, but that the signal intensity of cyclin D1 staining in the GFP⁺ area was lower in Hbp1 overexpression and higher in *Hbp1* knockdown (Fig. 8B).

In line with the above findings, expression levels of cyclin D1 were strikingly upregulated and c-Jun expression was also upregulated in the cortical regions of *Hbp1* icKO mice at E12.5 and E14.5 (Fig. 8C,D). Double-labeling with Pax6 or Tbr2 revealed that enhanced cyclin D1 expression was observed in most NSCs and a subset of IPs (data not shown). Real-time RT-PCR confirmed the significant upregulation of *cyclin D1* expression in the icKO at E12.5 and E14.5 (Fig. 8E). The expression levels of *cyclin E1* (*Ccne1* – Mouse Genome Informatics) and *N-myc* were slightly upregulated and sustained until later stages in the icKO (supplementary material Fig. S7B). Immunohistochemistry using antibodies against phosphorylated Rb (p-Rb) (Ser 780, Ser 807/811), a major target of cyclin D1/Cdk4/6 complexes (Kitagawa et al., 1996; Zarkowska and Mittnacht, 1997; Ely et al., 2005), revealed that the proportions of M phase cells that were strongly positive for p-Rb (Ser 780) were significantly higher in both Pax6⁺ NSCs and Tbr2⁺ IPs in the mutant cortex at E12.5 and E14.5, and the signal intensity of p-Rb (Ser 807/811) was slightly higher throughout the VZ of icKO at E14.5 (supplementary material Fig. S8A,B). Western blot analysis revealed the increased levels of p-Rb (Ser 807/811) in the mutant cortex at E14.5 (supplementary material Fig. S8C,D).

Cyclin D1 is a crucial factor involved in the regulation of cell cycle length by Hbp1

To address whether the upregulation of cyclin D1 is causative of the phenotype of *Hbp1* deficiency, we performed rescue experiments by co-transfecting *shHbp1* and knockdown vectors against *cyclin D1* (*shCcnd1*) by *in utero* electroporation (supplementary material Fig. S9A,B). We introduced a mixture of *shHbp1* and *shCcnd1* at ratios of 3:1, 1:1 or 1:3, and found that co-transfection of *shCcnd1* rescued the shortening of cell cycle caused by *Hbp1* knockdown (Fig. 8F). However, the co-expression of *shCcnd1* could not rescue the effects of *Hbp1* knockdown on neuronal differentiation/ migration (supplementary material Fig. S9C,D), suggesting that Hbp1 has crucial functions not only in the regulation of cyclin D1 but also in the regulation of neuronal differentiation.

We then performed real-time RT-PCR using total RNAs prepared from NSCs in the embryonic cortex of *pHes1-d2EGFP* transgenic mice and found that *cyclin D1* expression was downregulated threefold between E11.5 and E13.5 (Fig. 8G). Intriguingly, the temporal dynamics of *cyclin D1* expression exhibited a striking contrast to *Hbp1* expression (see Fig. 1C). We further performed a reporter assay using a *cyclin D1* promoter (3.3 kb)-luciferase construct. Expression of Hbp1 by co-transfection of *pCAG-HA-Hbp1* vectors in HEK293T cells significantly repressed the *cyclin D1* promoter activity (Fig. 8H).

Collectively, these data suggest that upregulation of cyclin D1 caused active proliferation with a short cell cycle length in neural stem/progenitor cells in the developing cortex of *Hbp1*-deficient

Fig. 7. Enhanced cell cycle progression due to *Hbp1* deficiency. (A) Detection of incorporated EdU by a fluorogenic click reaction and immunolabeling using anti-Ki67 and anti-pH3 antibodies on coronal sections of the cortical regions at E14.5. EdU was administered intraperitoneally to pregnant mice 30 min before sacrifice. The boxed areas are shown in higher magnification on the right. (B) Graphs showing the numbers of EdU$^+$, Ki67$^+$ or pH3$^+$ cells within a radial column of 200 μm width in the middle part of dorsolateral telencephalon. (C) The proportions of proliferating (EdU$^+$) and mitotic (pH3$^+$) cells in either Pax6$^+$ or Tbr2$^+$ population at E14.5. (D-F) Estimation of the cell cycle length in whole proliferating cells (Ki67$^+$), NSCs (Pax6$^+$) or IPs (Tbr2$^+$) in the cortical regions by the BrdU/EdU double-labeling method. (G) Schematic demonstrating the relationship between the gradual elongation of cell cycle length and the timing of the transition from symmetric proliferative to asymmetric neurogenic division based on our observations. n=3, error bars: s.e.m.; *P<0.05, **P<0.01, ***P<0.001; Student's t-test; N.S., not significant. Scale bar: 200 μm.

mice, and that cyclin D1 is a crucial factor involved in the regulation of cell cycle length by Hbp1 during cortical development.

DISCUSSION
Rapid proliferation of NSCs delays the onset of neurogenesis
In the developing embryonic cortex, NSCs gradually alter their characteristics and give birth to distinct cell types in a precise temporal order (McConnell, 1989; Temple, 2001; Ohtsuka et al., 2011). In particular, the timing of the transition from symmetric proliferative to asymmetric neurogenic division is crucial in determining the onset of neurogenesis and the size of the initial stem cell pool. One possible mechanism underlying regulation of the timing of this transition is that the number of cell divisions intrinsically functions as a biological clock to determine their competence and to mark developmental steps in NSCs. If so,

rapid proliferation of NSCs with a shorter cell cycle will result in a precocious transition from symmetric to asymmetric division and an early onset of neurogenesis. An alternative possibility is that the gradual elongation of cell cycle length in NSCs during cortical development allows determinants for neuronal differentiation to accumulate to the threshold level that initiates asymmetric neurogenic division and thus acts as a regulator of the biological clock (Calegari and Huttner, 2003; Calegari et al., 2005; Götz and Huttner, 2005; Dehay and Kennedy, 2007). If this is the case, rapid cycling of NSCs inhibits these determinants from reaching the threshold needed to drive neuronal differentiation.

Our data support the latter hypothesis, because rapidly proliferating NSCs in the cortex of *Hbp1* icKO mice were maintained as cycling NSCs, and the generation of Tbr2$^+$ IPs and neurons was delayed (Fig. 4A-C and Fig. 5A,B). Our results suggest
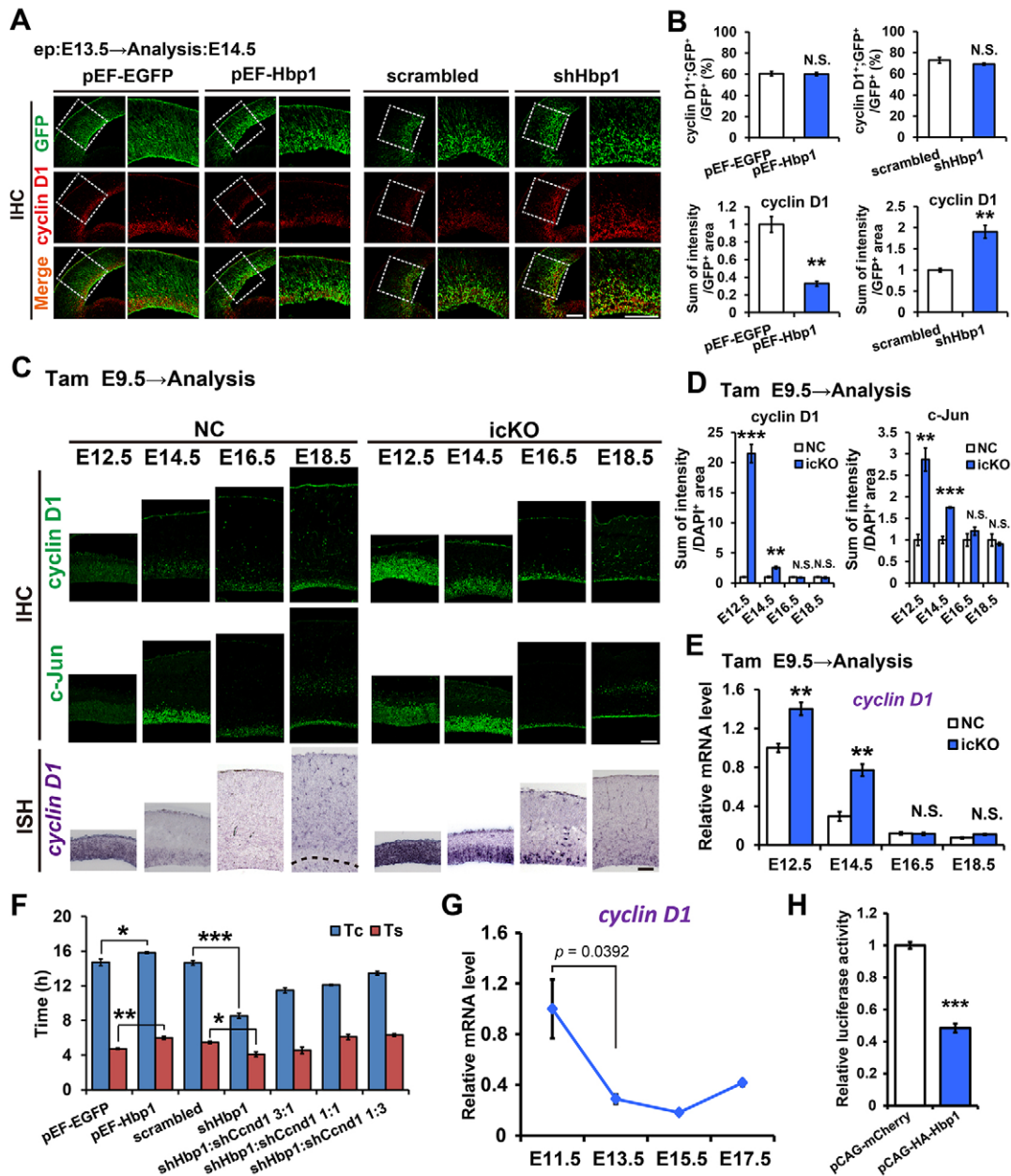
Fig. 8. Altered expression of cell cycle-related genes under modified Hbp1 expression levels. (A,C) Immunohistochemistry (for *cyclin D1* and c-Jun) and *in situ* hybridization (for *cyclin D1*) on coronal brain sections from mice subjected to overexpression or knockdown of Hbp1 (A) or in the *Hbp1* icKO mice (C). The boxed areas are shown in higher magnification on the right in A. Dashed line indicates the ventricular surface in C. (B) Graphs showing the proportions of cyclin D1$^+$ cells of GFP$^+$ cells and the signal intensity of cyclin D1 in the GFP$^+$ area at E14.5. (D) Graphs showing the signal intensity of cyclin D1 and c-Jun in DAPI$^+$ nuclei in the dorsolateral telencephalon. (E) Real-time RT-PCR using total RNAs prepared from the telencephalon to compare the expression levels of *cyclin D1* in the control and the icKO mice. *β-actin* was used as internal control, and the values were normalized to that of the E12.5 NC sample. (F) *pEF-EGFP*, *pEF-Hbp1*, scrambled shRNA, *shHbp1* and various combinations of *shHbp1* with *shCcnd1* were introduced into ventricular cells by *in utero* electroporation at E13.5, and the cell cycle length was estimated at E14.5 by the BrdU/EdU double-labeling method. (G) Real-time RT-PCR using total RNAs prepared from NSCs in the cortical regions of *pHes1-d2EGFP* transgenic mice showing the temporal dynamics of *cyclin D1* expression. *β-actin* was used as internal control, and the values were normalized to that of the E11.5 sample. (H) Reporter assay using a *cyclin D1* promoter (3.3 kb)-luciferase construct. This reporter construct and Hbp1 expression vectors (*pCAG-HA-Hbp1*) or control vectors (*pCAG-mCherry*) were co-transfected in HEK293T cells, and the luciferase activity was measured 48 h later. *n*=3, error bars: s.e.m.; *P<0.05, **P<0.01, ***P<0.001; Student's *t*-test; N.S., not significant. Scale bars: 200 μm in A; 100 μm in C.

that Hbp1 is required to elongate the cell cycle length and facilitate the attainment of the threshold length required to commence neurogenesis, as illustrated in Fig. 7G.

As observed in the mutant cortex at later stages, when NSC proliferation shifted to the asymmetric neurogenic division mode, the aberrantly rapid cell cycle accelerated the production of Tbr2$^+$

IPs and their proliferation in the SVZ. This resulted in the premature exhaustion of the neural stem/progenitor cell pool, rendering the neurogenic period shorter in the *Hbp1*-deficient mice. This raises the possibility that the number of cell divisions in neural stem/progenitor cells is intrinsically limited after the transition to the neurogenic mode.

Hbp1 inhibits cell cycle progression by suppressing cyclin D1 expression

Our observations revealed that *Hbp1* knockdown and *Hbp1*-deficiency led to cyclin D1 upregulation and accelerated cell cycle progression in neural stem/progenitor cells in the cortical regions, where reduction in T_C was more substantial than reduction in T_S (Fig. 7D-F and Fig. 8F). Given that cyclin D1 is required for the G1/S transition and that the durations of the G2 and M phases are relatively constant in distinct cell types, it is likely that T_{G1} was mainly reduced via upregulation of cyclin D1. Indeed, the primary phenotypes observed in the *Hbp1*-deficient mice were consistent with the cyclin D1 overexpression phenotype, in which T_{G1} was shortened, and inhibition of neurogenesis and expansion of IPs were observed (Lange et al., 2009; Pilaz et al., 2009).

It has been reported that T_C in neural progenitors is gradually elongated as development proceeds and is approximately doubled over the period between E11 and E15, mostly due to the elongation of T_{G1} (Miyama et al., 1997). Here, we found contrasting expression dynamics between *Hbp1* and *cyclin D1* in NSCs over the course of cortical development (Fig. 1C and Fig. 8G), and revealed that Hbp1 repressed the *cyclin D1* promoter activity (Fig. 8H). Together, these findings support our model that Hbp1 is involved in the elongation of T_{G1} in NSCs during early cortical development by regulating the expression of growth regulatory genes, including *cyclin D1*. Future genome-wide expression analysis comparing gene expression in the wild-type and *Hbp1*-deficient cortex will provide new insights into novel targets or effectors of Hbp1.

Rb1 cooperates with Hbp1 to promote terminal differentiation

It was speculated that Hbp1 induces cell cycle exit and promotes neuronal differentiation when overexpressed in neural stem/progenitor cells. However, overexpression of Hbp1 alone failed to promote terminal neuronal differentiation (Fig. 2A). We hypothesized that overexpression of Hbp1 alone would lead to cell cycle exit without tissue-specific gene expression, due to a low Rb1/Hbp1 ratio. We found that *Neurod1* expression was downregulated by Hbp1 overexpression (Fig. 2E) and that the repression was partly rescued by co-expression of Rb1, whereas expression of *Neurog2* was not significantly affected. It has been shown that Neurod1 regulates terminal neuronal differentiation (Lee et al., 1995; Schwab et al., 2000; Gao et al., 2009) and that Neurod1 expression is activated by the Wnt signaling in adult hippocampal neurogenesis (Kuwabara et al., 2009). Therefore, it is possible that overexpression of Hbp1 repressed *Neurod1* expression via inhibition of the Wnt signaling. We found that the expression levels of *Neurod1* were significantly upregulated in the cortex of *Hbp1*-deficient mice (Fig. 6A,B), suggesting that Hbp1 has a role in repressing *Neurod1* expression in neural stem/progenitor cells. Although it is likely that the cell cycle length was too short in the *Hbp1*-deficient mice for Neurog2 and Neurod1 to induce neuronal differentiation at earlier stages, the enhanced expression of these genes might have accelerated the production of Tbr2^{+} IPs after the transition to the asymmetric neurogenic division mode (Fig. 4A-C). Thus, our present study further corroborates the finding that Hbp1 promotes cell cycle exit but blocks terminal differentiation if the Rb1/Hbp1 ratio is low. Confirming this hypothesis, an increased ratio of Rb1/Hbp1 promoted terminal neuronal differentiation, similar to observations for muscle cell differentiation (Shih et al., 1998).

G1 elongation by Hbp1 is essential for cortical development

We previously reported that expression of the bHLH transcriptional repressor Hes1 is oscillatory with a period of 2-3 h in neural stem/progenitor cells in the developing cortex, and that expression of neurogenic bHLH genes such as *Neurog2* and *Ascl1* is also oscillating (Shimojo et al., 2008, 2011; Imayoshi et al., 2013). Thus, it is likely that some neurogenic bHLH factors or their downstream effectors gradually accumulate during the phase of oscillation when Hes1 expression is low. If the G1 phase is elongated, such determinants have a greater chance to reach the threshold necessary to exert their neurogenic functions. Therefore, it is presumed that the duration of the G1 phase is crucial in determining the onset of cortical neurogenesis.

Increases in the number of cell divisions during the symmetric proliferative division phase will cause the exponential expansion of NSCs as neuroepithelial cells (a non-neurogenic form of NSCs) and the increase in radial units composed of each stem cell and its progeny, thus leading to expansion of brain vesicles/ventricles and tangential extension of the VZ (Noctor et al., 2001). Once NSCs shift to the asymmetric neurogenic division mode, they transform into radial glial cells (a neurogenic form of NSCs), and the number of NSCs does not increase any further. Our findings demonstrate that in the absence of *Hbp1* neuroepithelial cells continued to proliferate rapidly by symmetric proliferative divisions and expanded the neuroepithelial sheet, leading to the expansion of the ventricular surface and the VZ.

Taken together, our results indicate that the elongation of cell cycle length by Hbp1 mediated by repression of cyclin D1 is a key mechanism regulating the proper timing of neuronal differentiation. As such, Hbp1 is a key factor in determining the onset of cortical neurogenesis and the duration of neurogenic period, thus being essential for normal cortical development.

MATERIALS AND METHODS

In situ hybridization

Preparation of digoxigenin-labeled antisense RNA probes and *in situ* hybridization were performed as described previously (Ohtsuka et al., 2011). We used partial-length cDNA of *Neurog2* (NM_009718.2) (0.87 kb) and full-length coding sequence of *Hbp1* (NM_153198.2), *Neurod1* (NM_010894.2), *Ascl1* (NM_008553.4), *Ccnd1* (NM_007631.2), *Ccne1* (NM_007633.2) and *Mycn* (NM_008709.3) as templates of the RNA probes.

Quantitative real-time RT-PCR

Total RNA samples were extracted from FACS-sorted embryonic NSCs prepared from the cortical regions of *pHes1-d2EGFP* transgenic mice as described previously (Ohtsuka et al., 2011). Reverse transcription of the total RNA and real-time RT-PCR were performed as previously described (Tan et al., 2012), using the primers listed in supplementary material Table S1. *β-actin* (*Actb*) was used as internal control.

Plasmid construction

For overexpression of *Hbp1*, full-length coding sequence of *Hbp1* (NM_153198.2) was cloned into the *pEF* (human elongation factor 1α promoter)-*MM* expression vector, which was modified from *pEF-BOS* vector (Mizushima and Nagata, 1990). The *pCAGGS-HA-hRb1* vector, in which HA (hemagglutinin)-tagged human *Rb1* was inserted into *pCAGGS* vector, was kindly provided by Dr Chiaki Takahashi and Dr Nobunari Sasaki (Kanazawa University, Japan). The *pCAG-HA-Hbp1* vector was created by inserting HA-tagged *Hbp1* into *pCAGEN* (Matsuda and Cepko, 2004). For the reporter assay, *Ccnd1* promoter region (from −3281 to +232) was inserted into *pGL4.10* (Promega), and the *Luc2* in *pGL4.10* was then replaced for the ubiquitylated luciferase fused with two nuclear localization sequences (*NLS2-Ub-Luc2*). For knockdown experiments, expression vectors were generated from annealed oligonucleotides

for shRNA targeting *Hbp1* (*shHbp1*) or *Ccnd1* (*shCcnd1*) (*Hbp1*: 5′-acct-cGGACTCTTCTGCGGTCTATGTtcaagagACATAGACCGCAGAAGA-GTCCtt-3′ and 5′-caaaaaGGACTCTTCTGCGGTCTATGTctcttgaACA-TAGACCGCAGAAGAGTCCg-3′; *Ccnd1*: 5′-acctcGTGCATCTACAC-TGACAACTtcaagagAGTTGTCAGTGTAGATGCACtt-3′ and 5′-caaaa-aGTGCATCTACACTGACAACTctcttgaAGTTGTCAGTGTAGATGCA-Cg-3′) inserted into the *Bbs*I site of psiRNA-h7SKneo G1 plasmid vector (InvivoGen), with the 20-21 nucleotide target sequence shown in uppercase letters, as described previously (Ohtsuka et al., 2011). Randomly scrambled sequence of the target was used for the negative control. The knockdown efficiency was confirmed in HEK293T cell lines.

In utero electroporation
Pregnant ICR mice were obtained from Japan SLC and CLEA Japan. *In utero* electroporation was performed with E13.5 ICR pregnant mice as described previously (Ohtsuka et al., 2011). All animals were handled in accordance with the Kyoto University Guide for the Care and Use of Laboratory Animals.

Immunohistochemistry
Immunohistochemistry was performed as described previously (Ohtsuka et al., 2011). The primary antibodies used are listed in supplementary material Table S2. Primary antibodies were detected with Alexa Fluor-conjugated secondary antibodies (1:200; Molecular Probes). To visualize the cell nuclei, 4′,6-diamidino-2-phenylindole (DAPI; Sigma-Aldrich) was added to slides. Fluorescent staining was analyzed with LSM510 and LSM780 confocal microscopes (Zeiss).

Analysis of cell cycle length
To estimate the cell cycle length, we conducted a dual-pulse-labeling of DNA synthesis using 5-bromo-2′-deoxyuridine (BrdU; Sigma-Aldrich) and 5-ethynyl-2′-deoxyuridine (EdU; Molecular Probes), referring to the previous methods (Martynoga et al., 2005; Mairet-Coello et al., 2012). Previous reports used EdU first, followed by BrdU, but here we administered BrdU first, followed by EdU. Using the anti-BrdU antibody MoBU-1 (Molecular Probes), we confirmed that the reverse order of injection produced the same results. BrdU (50 µg BrdU/g body weight) and EdU (12.5 µg EdU/g body weight) were injected intraperitoneally to the pregnant mice 2 h and 30 min before sacrifice, respectively, and the ratios of cells that incorporated either or both BrdU and EdU were analyzed to estimate the cell cycle length. The detection of EdU-labeled cells was performed based on a fluorogenic click reaction (Salic and Mitchison, 2008). Length of the S phase (T_S) and cell cycle length (T_C) were calculated as follows:

$$T_S = 1.5 \times S_{cells}/L_{cells} \ \ \text{and} \ \ T_C = T_S \times P_{cells}/S_{cells}$$

[L_{cells}, cells leaving S phase (identified as BrdU$^+$;EdU$^-$); S_{cells}, cells in S phase (EdU$^+$ only and double BrdU$^+$;EdU$^+$); P_{cells}, total proliferating cells (Ki67$^+$)].

Reporter assay
The luciferase reporter of *Ccnd1* (0.1 µg) and the expression plasmids (1.0 µg) were transfected into HEK293T cells. The *pRL-SV40* vector (1 ng; Promega) was co-transfected to normalize the transfection efficiency. Cells were harvested after 48 h and the reporter assay was performed as described previously (Sakamoto et al., 2003).

Statistical analysis
Each experiment was performed with at least three independent samples. Results are shown as mean±s.e.m. Statistical differences were examined with Student's *t*-test.

Supplementary material
Supplementary material available online at
http://dev.biologists.org/lookup/suppl/doi:10.1242/dev.120477/-/DC1

References
Artegiani, B., Lindemann, D. and Calegari, F. (2011). Overexpression of cdk4 and cyclinD1 triggers greater expansion of neural stem cells in the adult mouse brain. *J. Exp. Med.* **208**, 937-948.

Calegari, F. and Huttner, W. B. (2003). An inhibition of cyclin-dependent kinases that lengthens, but does not arrest, neuroepithelial cell cycle induces premature neurogenesis. *J. Cell Sci.* **116**, 4947-4955.

Calegari, F., Haubensak, W., Haffner, C. and Huttner, W. B. (2005). Selective lengthening of the cell cycle in the neurogenic subpopulation of neural progenitor cells during mouse brain development. *J. Neurosci.* **25**, 6533-6538.

Caviness, V. S., Jr, Goto, T., Tarui, T., Takahashi, T., Bhide, P. G. and Nowakowski, R. S. (2003). Cell output, cell cycle duration and neuronal specification: a model of integrated mechanisms of the neocortical proliferative process. *Cereb. Cortex* **13**, 592-598.

Dehay, C. and Kennedy, H. (2007). Cell-cycle control and cortical development. *Nat. Rev. Neurosci.* **8**, 438-450.

Delalle, I., Takahashi, T., Nowakowski, R. S., Tsai, L.-H. and Caviness, V. S., Jr. (1999). Cyclin E-p27 opposition and regulation of the G1 phase of the cell cycle in the murine neocortical PVE: a quantitative analysis of mRNA in situ hybridization. *Cereb. Cortex* **9**, 824-832.

Elfert, S., Weise, A., Bruser, K., Biniossek, M. L., Jägle, S., Senghaas, N. and Hecht, A. (2013). Acetylation of human TCF4 (TCF7L2) proteins attenuates inhibition by the HBP1 repressor and induces a conformational change in the TCF4::DNA complex. *PLoS ONE* **8**, e61867.

Ely, S., Di Liberto, M., Niesvizky, R., Baughn, L. B., Cho, H. J., Hatada, E. N., Knowles, D. M., Lane, J. and Chen-Kiang, S. (2005). Mutually exclusive cyclin-dependent kinase 4/cyclin D1 and cyclin-dependent kinase 6/cyclin D2 pairing inactivates retinoblastoma protein and promotes cell cycle dysregulation in multiple myeloma. *Cancer Res.* **65**, 11345-11353.

Gao, Z., Ure, K., Ables, J. L., Lagace, D. C., Nave, K.-A., Goebbels, S., Eisch, A. J. and Hsieh, J. (2009). Neurod1 is essential for the survival and maturation of adult-born neurons. *Nat. Neurosci.* **12**, 1090-1092.

Gartel, A. L., Goufman, E., Tevosian, S. G., Shih, H., Yee, A. S. and Tyner, A. L. (1998). Activation and repression of p21(WAF1/CIP1) transcription by RB binding proteins. *Oncogene* **17**, 3463-3469.

Götz, M. and Huttner, W. B. (2005). The cell biology of neurogenesis. *Nat. Rev. Mol. Cell Biol.* **6**, 777-788.

Imayoshi, I., Isomura, A., Harima, Y., Kawaguchi, K., Kori, H., Miyachi, H., Fujiwara, T., Ishidate, F. and Kageyama, R. (2013). Oscillatory control of factors determining multipotency and fate in mouse neural progenitors. *Science* **342**, 1203-1208.

Kim, J., Zhang, X., Rieger-Christ, K. M., Summerhayes, I. C., Wazer, D. E., Paulson, K. E. and Yee, A. S. (2006). Suppression of Wnt signaling by the green tea compound (-)-epigallocatechin 3-gallate (EGCG) in invasive breast cancer cells: requirement of the transcriptional repressor HBP1. *J. Biol. Chem.* **281**, 10865-10875.

Kitagawa, M., Higashi, H., Jung, H. K., Suzuki-Takahashi, I., Ikeda, M., Tamai, K., Kato, J., Segawa, K., Yoshida, E., Nishimura, S. et al. (1996). The consensus motif for phosphorylation by cyclin D1-Cdk4 is different from that for phosphorylation by cyclin A/E-Cdk2. *EMBO J.* **15**, 7060-7069.

Kuwabara, T., Hsieh, J., Muotri, A., Yeo, G., Warashina, M., Lie, D. C., Moore, L., Nakashima, K., Asashima, M. and Gage, F. H. (2009). Wnt-mediated activation of NeuroD1 and retro-elements during adult neurogenesis. *Nat. Neurosci.* **12**, 1097-1105.

Lange, C., Huttner, W. B. and Calegari, F. (2009). Cdk4/cyclinD1 overexpression in neural stem cells shortens G1, delays neurogenesis, and promotes the generation and expansion of basal progenitors. *Cell Stem Cell* **5**, 320-331.

Lee, J. E., Hollenberg, S. M., Snider, L., Turner, D. L., Lipnick, N. and Weintraub, H. (1995). Conversion of Xenopus ectoderm into neurons by NeuroD, a basic helix-loop-helix protein. *Science* **268**, 836-844.

Mairet-Coello, G., Tury, A., Van Buskirk, E., Robinson, K., Genestine, M. and DiCicco-Bloom, E. (2012). p57(KIP2) regulates radial glia and intermediate precursor cell cycle dynamics and lower layer neurogenesis in developing cerebral cortex. *Development* **139**, 475-487.

Martynoga, B., Morrison, H., Price, D. J. and Mason, J. O. (2005). Foxg1 is required for specification of ventral telencephalon and region-specific regulation of dorsal telencephalic precursor proliferation and apoptosis. *Dev. Biol.* **283**, 113-127.

Matsuda, T. and Cepko, C. L. (2004). Electroporation and RNA interference in the rodent retina in vivo and in vitro. *Proc. Natl. Acad. Sci. USA* **101**, 16-22.

McConnell, S. K. (1989). The determination of neuronal fate in the cerebral cortex. *Trends Neurosci.* **12**, 342-349.

Miyama, S., Takahashi, T., Nowakowski, R. S. and Caviness, V. S., Jr. (1997). A gradient in the duration of the G1 phase in the murine neocortical proliferative epithelium. *Cereb. Cortex* **7**, 678-689.

Mizushima, S. and Nagata, S. (1990). pEF-BOS, a powerful mammalian expression vector. *Nucleic Acids Res.* **18**, 5322.

Noctor, S. C., Flint, A. C., Weissman, T. A., Dammerman, R. S. and Kriegstein, A. R. (2001). Neurons derived from radial glial cells establish radial units in neocortex. *Nature* **409**, 714-720.

Ohtsuka, T., Imayoshi, I., Shimojo, H., Nishi, E., Kageyama, R. and McConnell, S. K. (2006). Visualization of embryonic neural stem cells using Hes promoters in transgenic mice. *Mol. Cell. Neurosci.* **31**, 109-122.

Ohtsuka, T., Shimojo, H., Matsunaga, M., Watanabe, N., Kometani, K., Minato, N. and Kageyama, R. (2011). Gene expression profiling of neural stem cells and identification of regulators of neural differentiation during cortical development. *Stem Cells* **29**, 1817-1828.

Pilaz, L.-J., Patti, D., Marcy, G., Ollier, E., Pfister, S., Douglas, R. J., Betizeau, M., Gautier, E., Cortay, V., Doerflinger, N. et al. (2009). Forced G1-phase reduction alters mode of division, neuron number, and laminar phenotype in the cerebral cortex. *Proc. Natl. Acad. Sci. USA* **106**, 21924-21929.

Sakamoto, M., Hirata, H., Ohtsuka, T., Bessho, Y. and Kageyama, R. (2003). The basic helix-loop-helix genes Hesr1/Hey1 and Hesr2/Hey2 regulate maintenance of neural precursor cells in the brain. *J. Biol. Chem.* **278**, 44808-44815.

Salic, A. and Mitchison, T. J. (2008). A chemical method for fast and sensitive detection of DNA synthesis in vivo. *Proc. Natl. Acad. Sci. USA* **105**, 2415-2420.

Sampson, E. M., Haque, Z. K., Ku, M.-C., Tevosian, S. G., Albanese, C., Pestell, R. G., Paulson, K. E. and Yee, A. S. (2001). Negative regulation of the Wnt-beta-catenin pathway by the transcriptional repressor HBP1. *EMBO J.* **20**, 4500-4511.

Schwab, M. H., Bartholomae, A., Heimrich, B., Feldmeyer, D., Druffel-Augustin, S., Goebbels, S., Naya, F. J., Zhao, S., Frotscher, M., Tsai, M. J. et al. (2000). Neuronal basic helix-loop-helix proteins (NEX and BETA2/Neuro D) regulate terminal granule cell differentiation in the hippocampus. *J. Neurosci.* **20**, 3714-3724.

Sessa, A., Mao, C.-A., Hadjantonakis, A.-K., Klein, W. H. and Broccoli, V. (2008). Tbr2 directs conversion of radial glia into basal precursors and guides neuronal amplification by indirect neurogenesis in the developing neocortex. *Neuron* **60**, 56-69.

Shih, H. H., Tevosian, S. G. and Yee, A. S. (1998). Regulation of differentiation by HBP1, a target of the retinoblastoma protein. *Mol. Cell. Biol.* **18**, 4732-4743.

Shih, H. H., Xiu, M., Berasi, S. P., Sampson, E. M., Leiter, A., Paulson, K. E. and Yee, A. S. (2001). HMG box transcriptional repressor HBP1 maintains a proliferation barrier in differentiated liver tissue. *Mol. Cell. Biol.* **21**, 5723-5732.

Shimojo, H., Ohtsuka, T. and Kageyama, R. (2008). Oscillations in notch signaling regulate maintenance of neural progenitors. *Neuron* **58**, 52-64.

Shimojo, H., Ohtsuka, T. and Kageyama, R. (2011). Dynamic expression of notch signaling genes in neural stem/progenitor cells. *Front. Neurosci.* **5**, 78.

Sun, Y., Nadal-Vicens, M., Misono, S., Lin, M. Z., Zubiaga, A., Hua, X., Fan, G. and Greenberg, M. E. (2001). Neurogenin promotes neurogenesis and inhibits glial differentiation by independent mechanisms. *Cell* **104**, 365-376.

Takahashi, T., Nowakowski, R. S. and Caviness, V. S., Jr. (1995). The cell cycle of the pseudostratified ventricular epithelium of the embryonic murine cerebral wall. *J. Neurosci.* **15**, 6046-6057.

Takahashi, T., Goto, T., Miyama, S., Nowakowski, R. S. and Caviness, V. S., Jr. (1999). Sequence of neuron origin and neocortical laminar fate: relation to cell cycle of origin in the developing murine cerebral wall. *J. Neurosci.* **19**, 10357-10371.

Tan, S.-L., Nishi, M., Ohtsuka, T., Matsui, T., Takemoto, K., Kamio-Miura, A., Aburatani, H., Shinkai, Y. and Kageyama, R. (2012). Essential roles of the histone methyltransferase ESET in the epigenetic control of neural progenitor cells during development. *Development* **139**, 3806-3816.

Temple, S. (2001). The development of neural stem cells. *Nature* **414**, 112-117.

Tevosian, S. G., Shih, H. H., Mendelson, K. G., Sheppard, K. A., Paulson, K. E. and Yee, A. S. (1997). HBP1: a HMG box transcriptional repressor that is targeted by the retinoblastoma family. *Genes Dev.* **11**, 383-396.

Yan, Z., Wang, J., Wang, C., Jiao, Y., Qi, W. and Che, S. (2014). miR-96/HBP1/Wnt/β-catenin regulatory circuitry promotes glioma growth. *FEBS Lett.* **588**, 3038-3046.

Zarkowska, T. and Mittnacht, S. (1997). Differential phosphorylation of the retinoblastoma protein by G1/S cyclin-dependent kinases. *J. Biol. Chem.* **272**, 12738-12746.

DEVELOPMENT

Supplementary Materials and Methods

Generation of *Hbp1* induced conditional knockout mice

The construction of targeting vector and gene targeting in *TT2* ES cell line were conducted as previously described (Imayoshi et al., 2013). For the generation of the targeting vector for FRT-neomycin-FRT cassette-inserted *Hbp1*-floxed mice, in which LoxP site and LoxP-FRT-neomycin-FRT cassette were inserted into intron 1 and 2 of *Hbp1* gene, respectively, BAC (bacterial artificial chromosome) carrying *Hbp1* genomic locus of the C57BL/6J background was purchased from BACPAC Resource Center (Children's Hospital Oakland Research Institute, Clone ID: RP23-193M19). For screening of successfully targeted ES cell clones, *Hbp1*-targeted allele (*Hbp1*-floxed-neo) was evaluated by Southern blot analysis of genomic DNA of the ES cells as described previously (Imayoshi et al., 2010). For preparing probes for Southern blot, PCR fragments amplified by using the primers listed in supplementary material Table S1 were cloned into pTA2 vector (TOYOBO), and the vectors were double-digested with *Cla*I and *Sal*I and then purified by electrophoresis and QIAquick Gel Extraction Kit (QIAGEN). After creating the chimeric mice carrying *Hbp1*-floxed-neo allele by using the ES cells obtained, we crossed them with *CAG-FLPe*$^{+/\Phi}$ mice (Kanki et al., 2006) to remove the neomycin cassette. PCR-based genotyping for *Hbp1*-floxed allele was performed using genomic DNA from mouse tails as a template. The specific primers used were listed in supplementary material Table S1. We generated *Hbp1*$^{flx/+}$ mice by removing CAG-FLPe transgene by crossing mice. By crossing them with *Nestin-CreER*^{T2} *L5-1*$^{+/\Phi}$ transgenic mice (Imayoshi et al., 2006), we obtained *Nestin-CreER*^{T2} *L5-1*$^{+/\Phi}$;*Hbp1*$^{flx/flx}$ mice. These mice were maintained on a mixed C57BL/6J and ICR background. For activation of CreER^{T2}, 5.2 mg of tamoxifen (Sigma-Aldrich) per 40 g of body weight was administered by oral gavage to the pregnant mice at E9.5 as described previously (Imayoshi et al., 2010). We used the tamoxifen-induced *Nestin-CreER*^{T2} *L5-1*$^{+/\Phi}$ mice as a negative control (NC).

Western blot analysis

HEK293T cells and the brains of embryos were disrupted and homogenized with lysis buffer [50 mM Tris-HCl pH 8.0, 100 mM NaCl, 5 mM MgCl$_2$, 0.5% NP-40, 1× Complete Proteinase Inhibitor Cocktail (Roche), 1 mM phenylmethanesulfonylfluoride, 250 U/ml Benzonase (Sigma-Aldrich)] and incubated on ice for 30 min before adding 1/10 volume

of 10% SDS to the lysates, and then the samples were boiled for 3 min. SDS-PAGE and Western blotting were performed as described previously (Harima et al. 2013). The primary antibodies used were listed in supplementary material Table S2.

Measurement

The signal intensity of the immunoreaction for anti-cyclin D1 antibody in GFP$^+$ area and DAPI$^+$ nuclei was analyzed by using the modules of "IdentifyPrimaryObjects", "MaskImage" and "MeasureImageIntensity" in CellProfiler 2.1.1 (Broad Institute). The measurement of the length and area was performed by using ImageJ 1.48 (Wayne Rasband, NIH, USA). The cell counting, including the counting of double and triple-positive cells, was conducted manually by using the plug-in of "Cell Counter" in ImageJ 1.48. For Pax6$^+$ cell counting in the lateral cortices, single-plane confocal images of coronal sections were obtained using motorized XY-scanning stage of LSM780 (Zeiss), and then the Pax6$^+$ fluorescence signals were counted automatically using the function of "Spots" in Imaris 7.6.5 (Bitplane). The number of Pax6$^+$ NSCs throughout the cortical regions in multiple coronal sections at constant intervals was summed up along the antero-posterior axis of lateral ventricle; thus the total number of NSCs in the hemisphere was estimated and compared between the control and icKO. In the scanned sections containing the ventricles, vesicle area, length of brain surface and ventricular surface of dorsolateral telencephalon, area of ventral telencephalon, and thickness of the VZ/SVZ/IZ+CP in the dorsolateral telencephalon were measured at the interval of 544 µm at E14.5.

References

Harima, Y., Takashima, Y., Ueda, Y., Ohtsuka, T. and Kageyama, R. (2013). Accelerating the tempo of the segmentation clock by reducing the number of introns in the Hes7 gene. *Cell Reports* 3, 1-7.

Imayoshi, I., Ohtsuka, T., Metzger, D., Chambon, P. and Kageyama, R. (2006). Temporal regulation of Cre recombinase activity in neural stem cells. *Genesis* 44, 233-238.

Imayoshi, I., Sakamoto, M., Yamaguchi, M., Mori, K. and Kageyama, R. (2010). Essential roles of Notch signaling in maintenance of neural stem cells in developing and adult brains. *J. Neurosci.* 30, 3489-3498.

Kanki, H., Suzuki, H. and Itohara, S. (2006). High-efficiency CAG-FLPe deleter mice in C57BL/6J background. *Exp. Anim.* 55, 137-141.
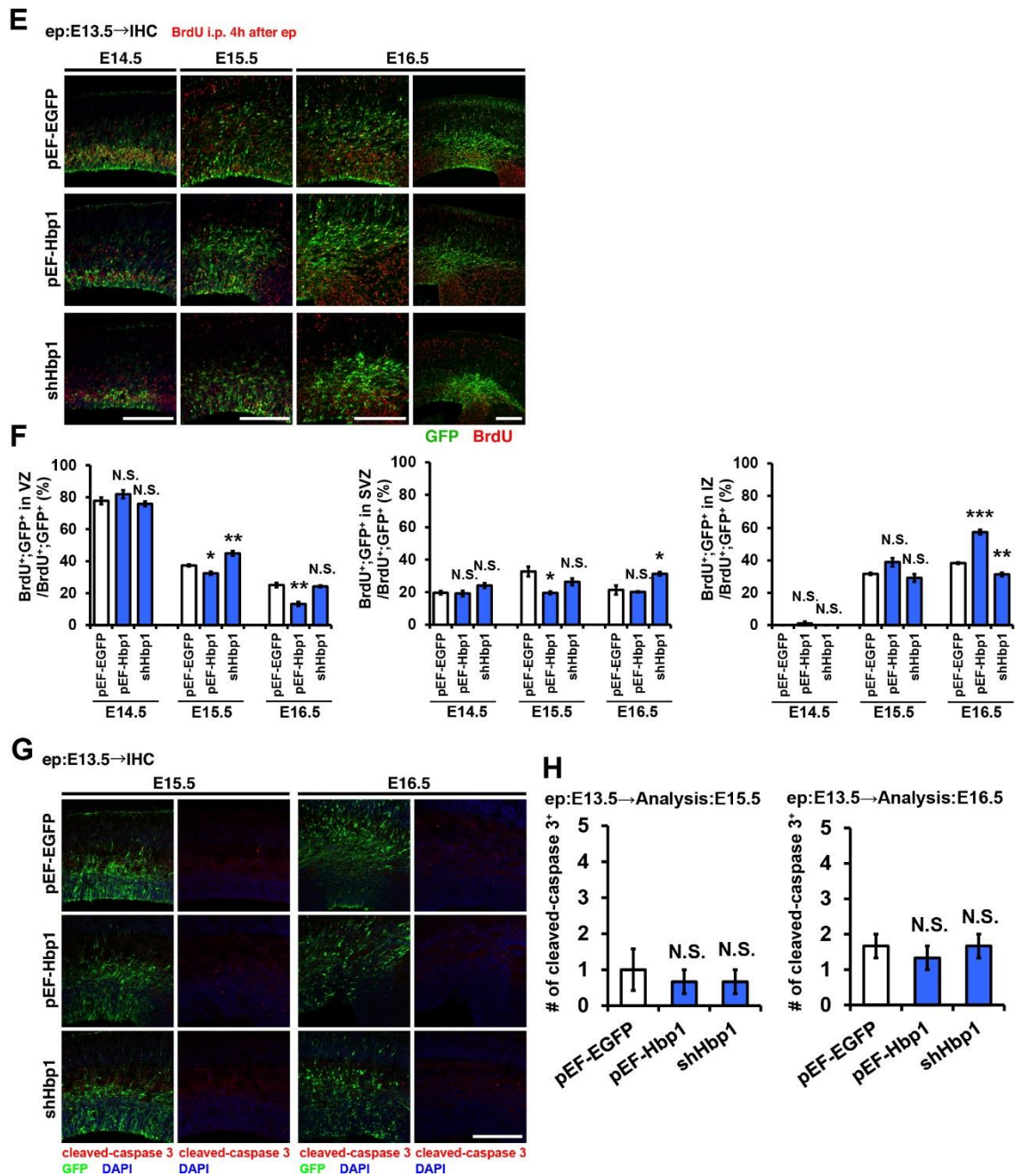
Figures
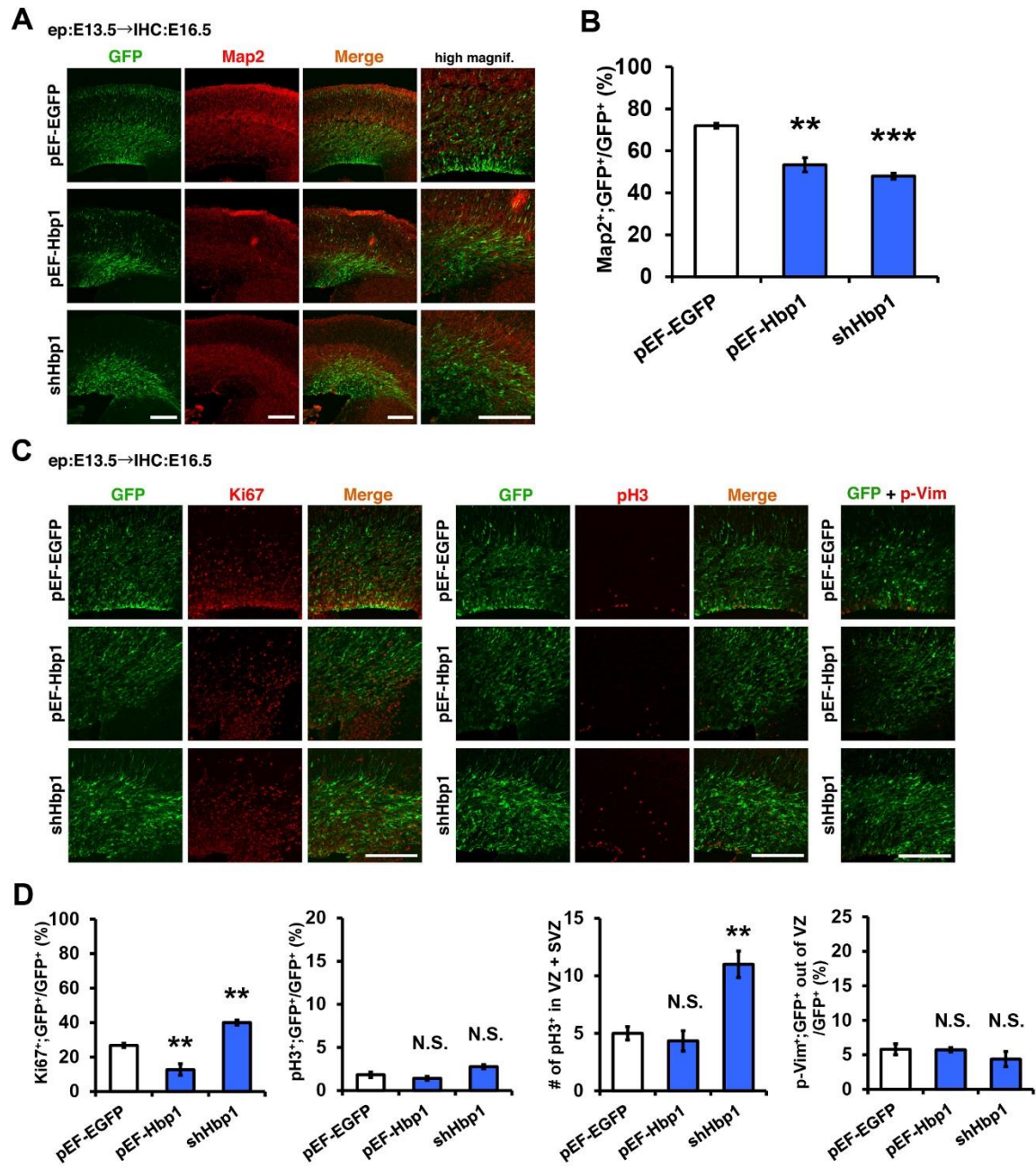
Fig. S1. Characterization of transfected cells in overexpression and knockdown experiments. *In utero* electroporation (ep) was performed with control vectors (*pEF-EGFP*) only or with a combination of *pEF-Hbp1* or *shHbp1* at E13.5, and the fates of transfected cells were analyzed by immunohistochemistry (IHC). (**A**) Coronal sections of dorsolateral telencephalon were double-stained using anti-GFP (green) and anti-Map2 (red) antibodies. (**B**) The proportions of Map2+ cells of transfected (GFP+) cells. (**C**) Double-staining using anti-GFP (green) and anti-Ki67/pH3/p-Vim (red)

antibodies. (**D**) The proportions of Ki67$^+$ or pH3$^+$ cells of transfected (GFP$^+$) cells, the numbers of pH3$^+$ cells in the VZ/SVZ within a radial column of 200 μm width, and the proportions of p-Vim$^+$;GFP$^+$ cells outside the VZ of GFP$^+$ cells. (**E**) BrdU was administered intraperitoneally to pregnant mice 4 h after *in utero* electroporation and sacrificed after 24 h at E14.5, 48 h at E15.5 and 72 h at E16.5. Coronal sections of dorsolateral telencephalon were double-stained using anti-GFP (green) and anti-BrdU (red) antibodies. (**F**) Graphs showing the proportions of BrdU$^+$;GFP$^+$ cells in the VZ, SVZ or IZ of total BrdU$^+$;GFP$^+$ cells. (**G**) Triple-staining using anti-GFP (green) and anti-cleaved-caspase 3 (red) antibodies and DAPI (blue) at E15.5 and E16.5. (**H**) The numbers of cleaved-caspase 3$^+$ cells within a radial column of 200 μm width. *n*=3, error bars: s.e.m.; *P<0.05, **P<0.01, ***P<0.001; Student's *t*-test; N.S., not significant. Scale bars: 200 μm.
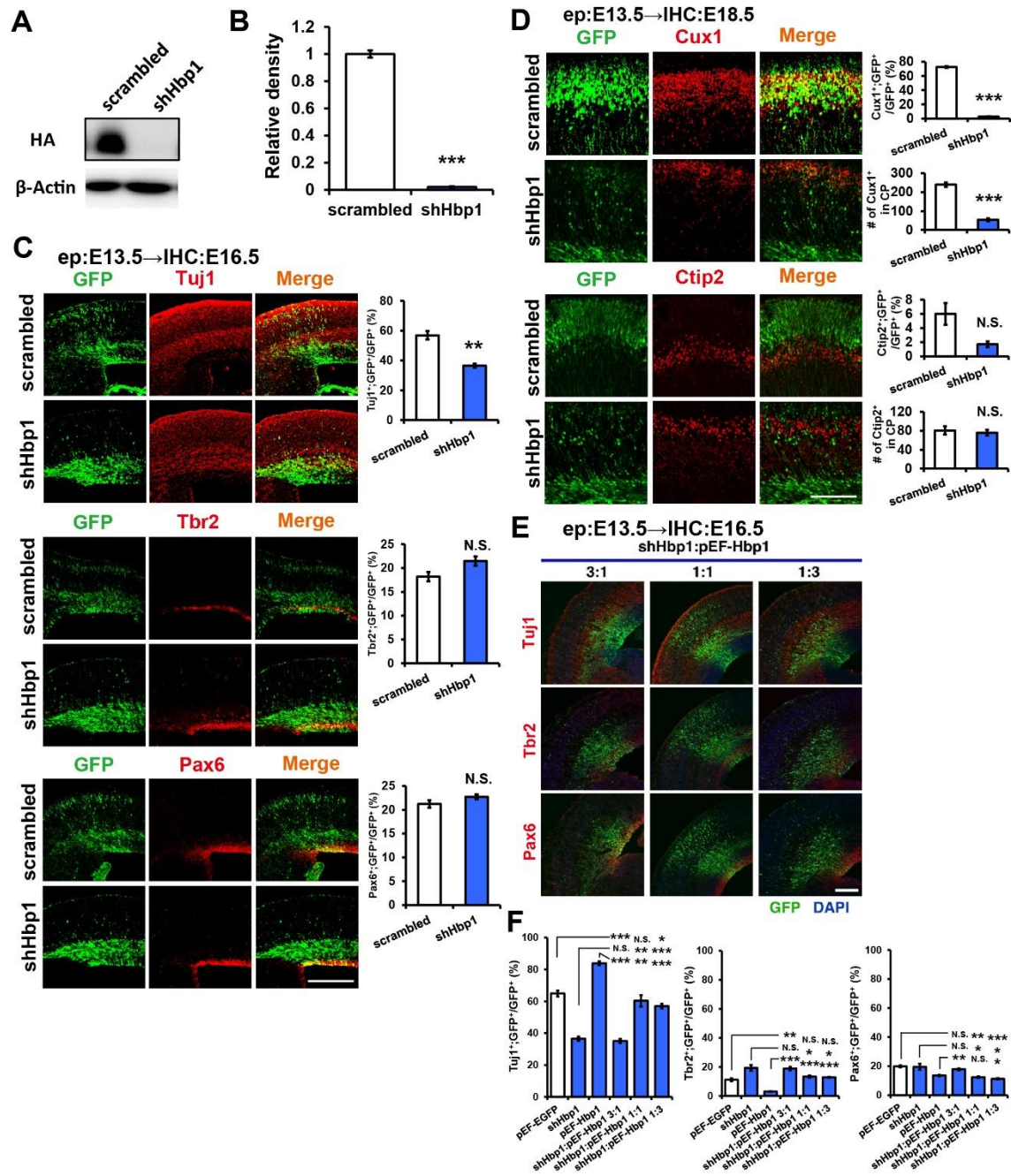
Fig. S2. Inhibition of neuronal differentiation by knockdown of *Hbp1*. (**A**) Knockdown efficiency of *shHbp1* was evaluated by western blot. HEK293T cells were co-transfected with expression vectors (*pEF-HA-Hbp1*) that express HA (hemagglutinin)-tagged Hbp1 and expression vectors of either shRNA targeting *Hbp1* (*shHbp1*) or scrambled shRNA control vectors (*scrambled*), and proteins were extracted from cells 24 h later. HA-Hbp1 protein was detected with anti-HA antibodies. (**B**) Expression levels of HA-Hbp1 protein in knockdown cells were estimated as 2.14 ±

0.00% compared with the control. β-Actin was used as an internal control, and the values were normalized to that in the control. (**C**,**D**) *shHbp1* or scrambled shRNA vectors were introduced into ventricular cells by *in utero* electroporation at E13.5. Coronal sections of dorsolateral telencephalon were immunostained to analyze the fates of transfected cells at E16.5 (C) or E18.5 (D). Anti-GFP (green) and anti-Tuj1/Tbr2/Pax6 (C) or anti-Cux1/Ctip2 (D) (red) antibodies were used for double-labeling. The proportions of cells positive for each marker (Tuj1, Tbr2 or Pax6) (C) and the proportions of Cux1$^+$ or Ctip2$^+$ cells (D) of the *Hbp1* knockdown or control cells, and the numbers of Cux1$^+$ or Ctip2$^+$ cells in the CP within a radial column of 200 μm width (D) were shown in bar graphs. (**E**) *pEF-Hbp1* vectors were co-introduced with *shHbp1* at ratios of 3:1, 1:1 or 1:3 by *in utero* electroporation at E13.5, and the fates of transfected cells were analyzed at E16.5. Coronal sections of dorsolateral telencephalon were stained using anti-GFP (green) and anti-Tuj1/Tbr2/Pax6 (red) antibodies and DAPI (blue). (**F**) Graphs showing the proportions of Tuj1$^+$, Tbr2$^+$ or Pax6$^+$ cells of transfected (GFP$^+$) cells. *n*=3, error bars: s.e.m.; **P*<0.05, ***P*<0.01, ****P*<0.001; Student's *t*-test; N.S., not significant. Scale bars: 200 μm.
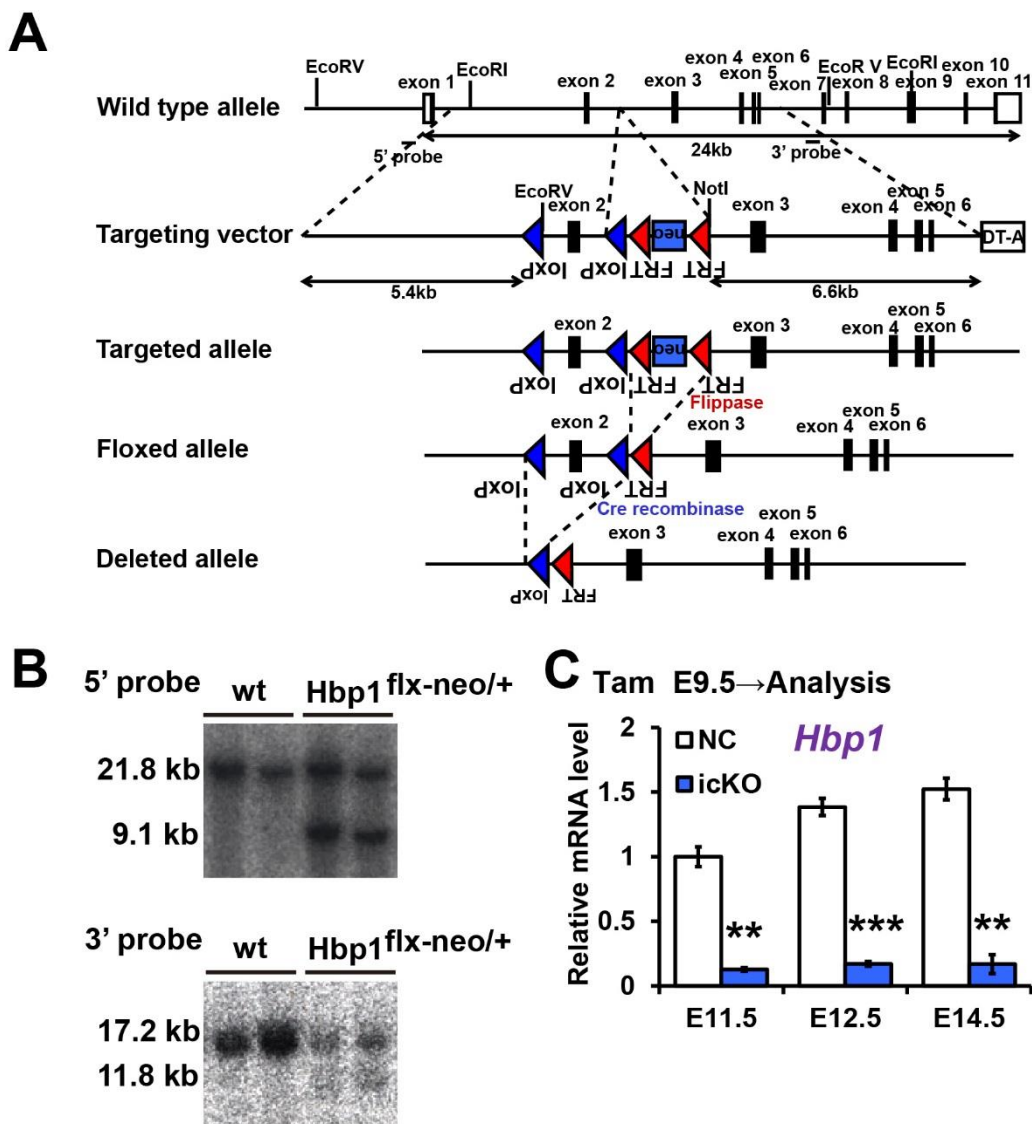
Fig. S3. Generation and validation of *Hbp1* icKO mice. (**A**) Schematic drawing of the strategy for generating *Hbp1* icKO mice. (**B**) Southern blot analysis of genomic DNA from wild-type and *Hbp1*-targeted ES cell clones by using *Eco*RV-digested DNA hybridized with 5' probe, which detected wild-type allele (wt): 21.8 kb and *Hbp1*-floxed-neo allele (flx-neo): 9.1 kb, and *Eco*RI and *Not*I-digested DNA hybridized with 3' probe, which detected wt: 17.2 kb and flx-neo: 11.8 kb. (**C**) Expression levels of *Hbp1* in the telencephalon of negative control (NC) and *Hbp1* icKO mice. Tamoxifen (Tam) was administered at E9.5, embryos were sacrificed at E11.5, E12.5 and E14.5, and real-time RT-PCR was performed using total RNAs prepared from the telencephalon. β-*actin* was used as internal control, and the values were normalized to that in NC at E11.5. *n*=3, error bars: s.e.m.; **$P<0.01$, ***$P<0.001$; Student's *t*-test.
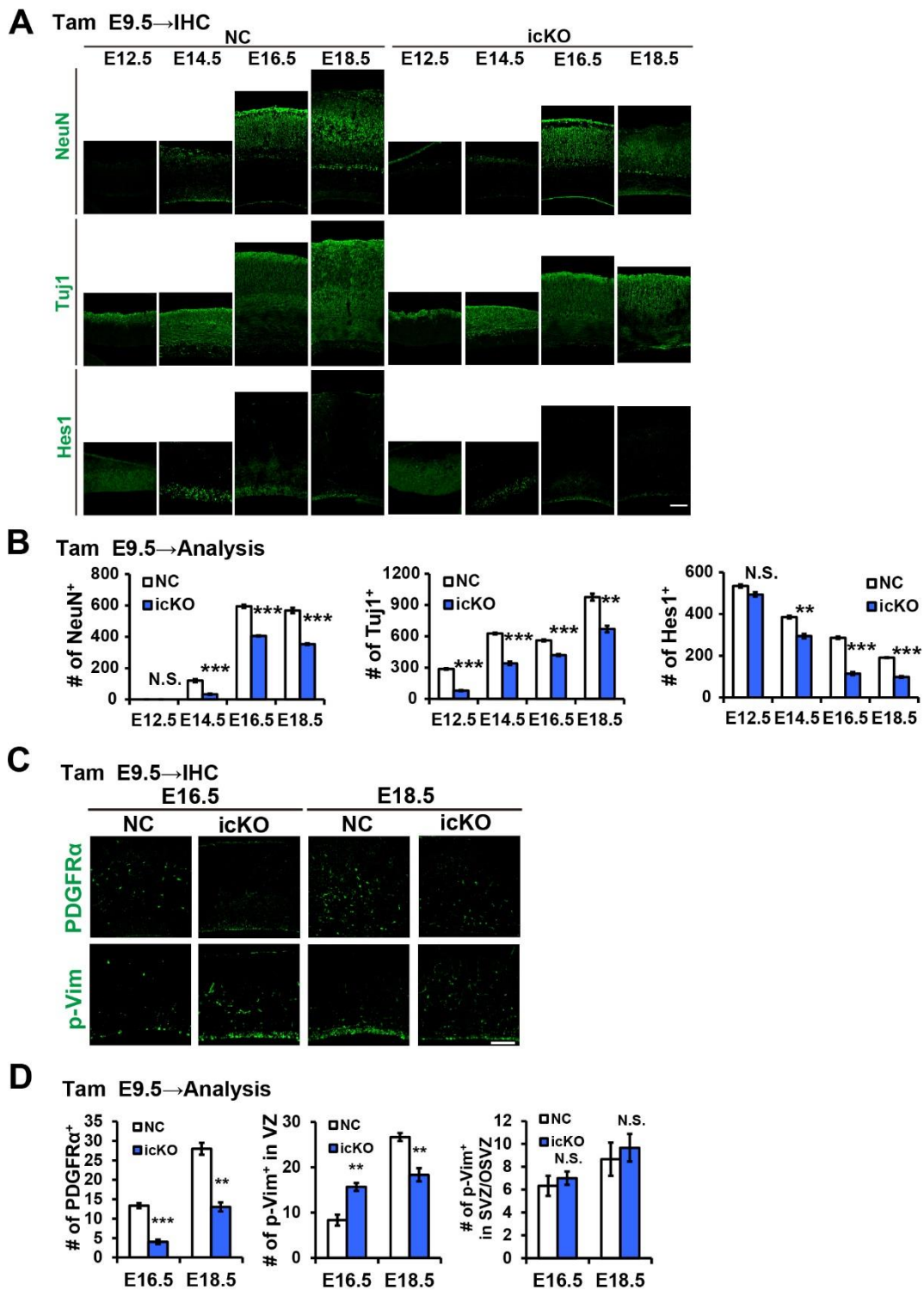
Fig. S4. Cortical development in *Hbp1*-deficient mice. (**A**) Immunohistochemistry on coronal sections of the cortical regions of control and *Hbp1* icKO mice at different developmental stages with neuronal markers such as NeuN and Tuj1, and Hes1, a marker for NSCs. (**B**) The number of cells immunoreactive for each antibody was

counted within a radial column of 200 μm width in the middle part of dorsolateral telencephalon. (**C**) Immunostaining on coronal sections of the cortical regions at E16.5 and E18.5 with antibodies against PDGFRα, a marker for oligodendrocyte precursor cells, and p-Vim, a marker for mitotic radial glial cells. (**D**) The numbers of PDGFRα$^+$ cells within a radial column of 200 μm width, and the numbers of p-Vim$^+$ cells in the VZ or SVZ/OSVZ within a radial column of 200 μm width. *n*=3, error bars: s.e.m.; **$P<0.01$, ***$P<0.001$; Student's *t*-test; N.S., not significant. Scale bars: 200 μm in A; 100 μm in C.
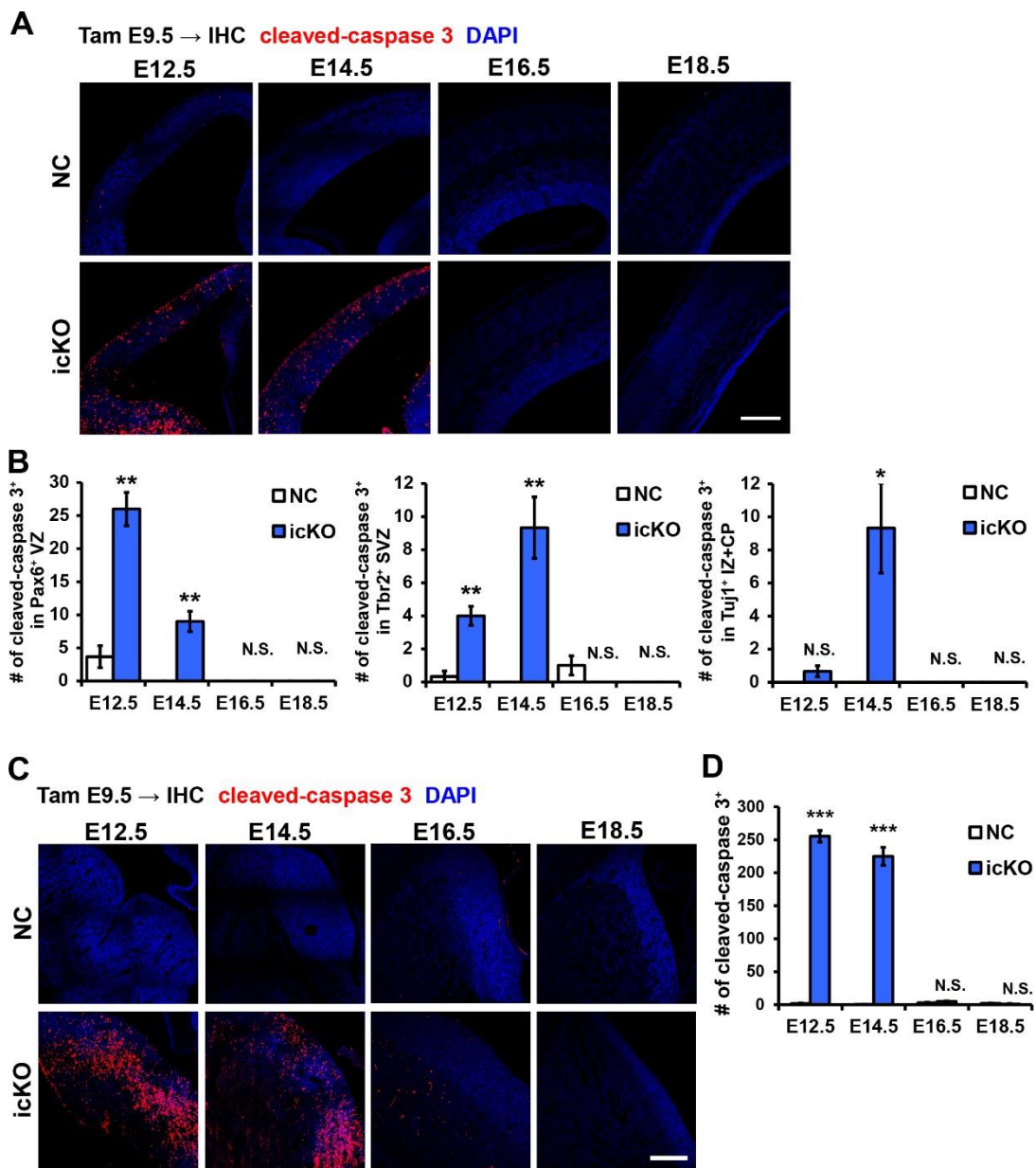
Fig. S5. Estimation of cell death in *Hbp1* icKO mice. (**A**) Cell death in neural stem/progenitor cells and neurons in the cortical regions of the control and the icKO was analyzed by immunohistochemistry using anti-cleaved-caspase 3 antibodies at different developmental stages. (**B**) The numbers of cleaved-caspase 3$^+$ cells in NSCs (Pax6$^+$), IPs (Tbr2$^+$) or neurons (Tuj1$^+$) in the control and the icKO embryos. (**C**) Analyses of cell death in the ventral telencephalon in the control and the icKO at different developmental stages. (**D**) The numbers of cleaved-caspase 3$^+$ cells within a 200 μm square in the ventral telencephalon. *n*=3, error bars: s.e.m.; *P<0.05, **P<0.01, ***P<0.001; Student's *t*-test; N.S., not significant. Scale bars: 200 μm.
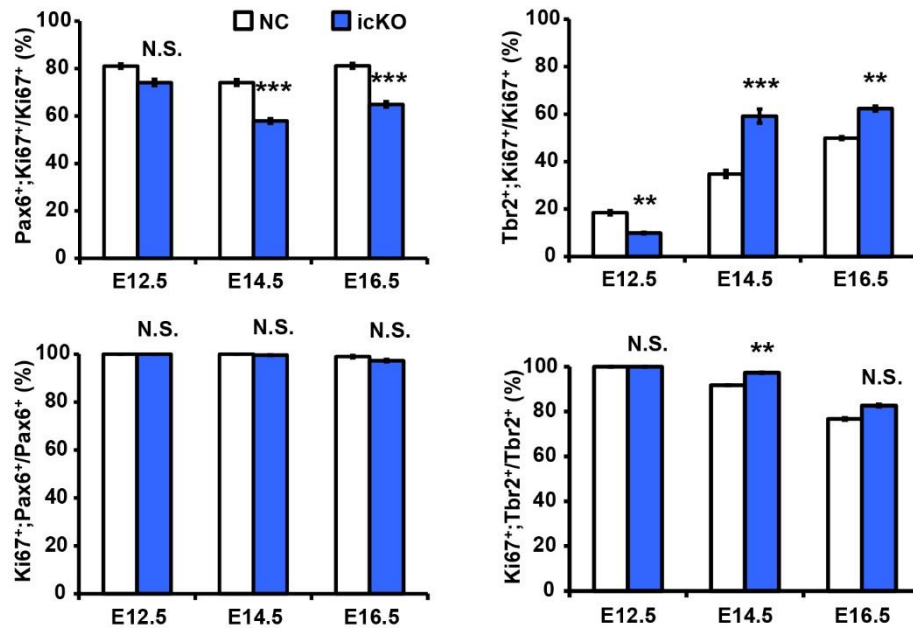
Fig. S6. Analysis of cell proliferation properties in *Hbp1* icKO mice. The proportions of Pax6^{+} or Tbr2^{+} cells of Ki67^{+} cells, and Ki67^{+} cells of Pax6^{+} or Tbr2^{+} cells in the cortical regions of the control and the icKO mice at different developmental stages. $n=3$, error bars: s.e.m.; **$P<0.01$, ***$P<0.001$; Student's *t*-test; N.S., not significant.
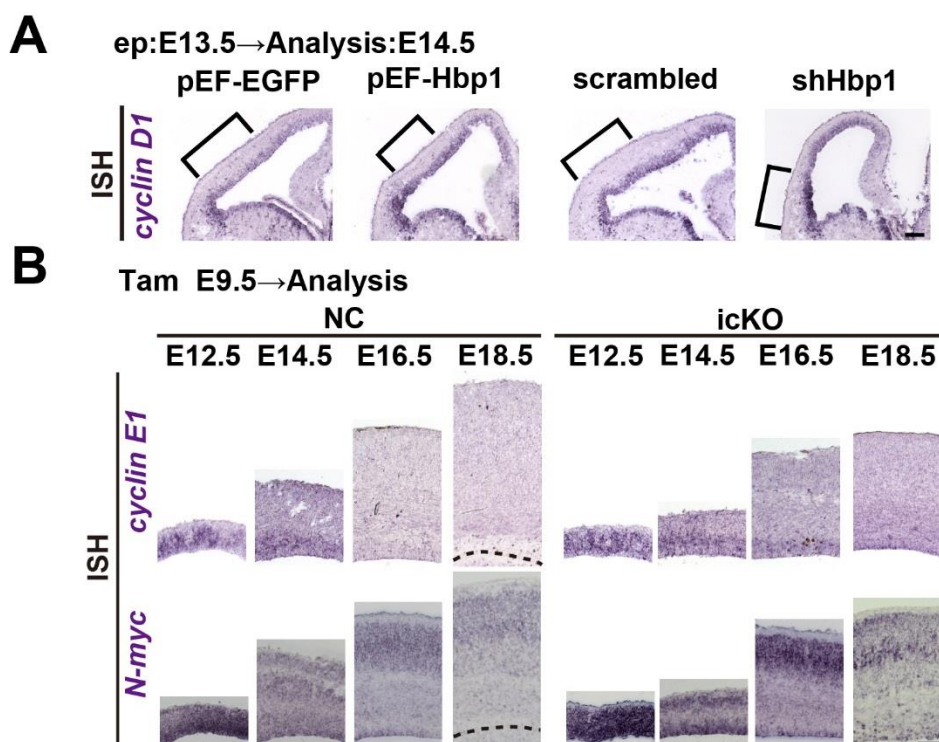
Fig. S7. Altered expression of cell cycle-related genes under modified Hbp1 expression levels. (**A**) *In situ* hybridization (ISH) for *cyclin D1* on coronal brain sections from mice subjected to overexpression or knockdown of Hbp1. Brackets indicate regions transfected with expression vectors. (**B**) *In situ* hybridization for *cyclin E1* and *N-myc* on coronal brain sections of the cortical regions of the control and the *Hbp1* icKO mice at different embryonic stages. Dashed lines indicate the ventricular surface. Scale bars: 200 μm in A; 100 μm in B.
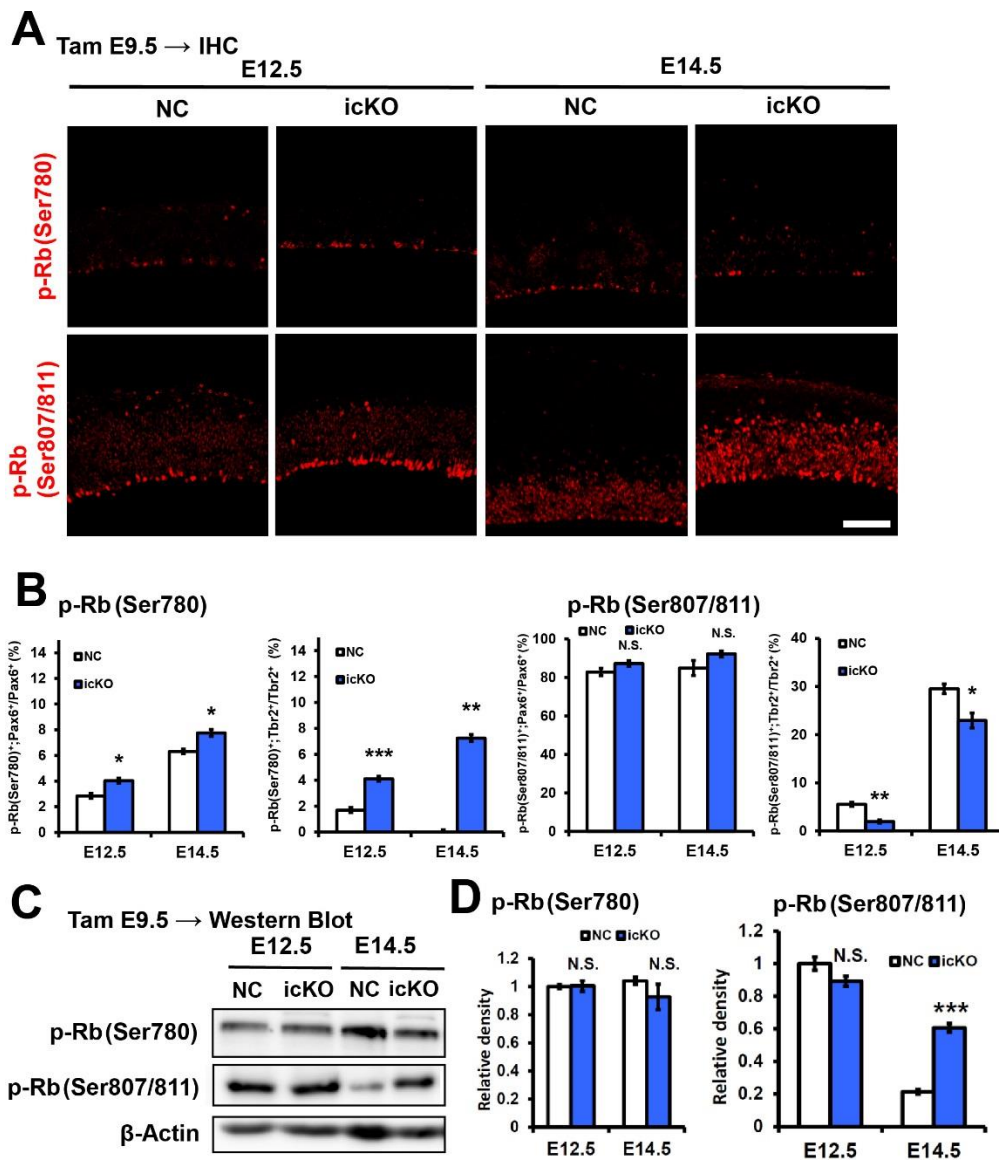
Fig. S8. Analysis of expression levels of phosphorylated Rb. (**A**) Immunohistochemistry showing the expression levels of phosphorylated Rb (p-Rb) (Ser 780, Ser 807/811) in the cortical regions of the control and the icKO mice at E12.5 and E14.5. (**B**) Graphs showing the proportions of p-Rb (Ser 780 or Ser 807/811) $^+$ cells of Pax6$^+$ or Tbr2$^+$ cells. (**C**) Western blot comparing the expression levels of p-Rb in the dorsolateral telencephalon of the control and the icKO mice at E12.5 and E14.5. (**D**) Graphs showing the expression levels of p-Rb protein. β-Actin was used as internal control, and the values were normalized to that in the control at E12.5. n=3, error bars: s.e.m.; *P<0.05, **P<0.01, ***P<0.001; Student's t-test; N.S., not significant. Scale bar: 100 μm.

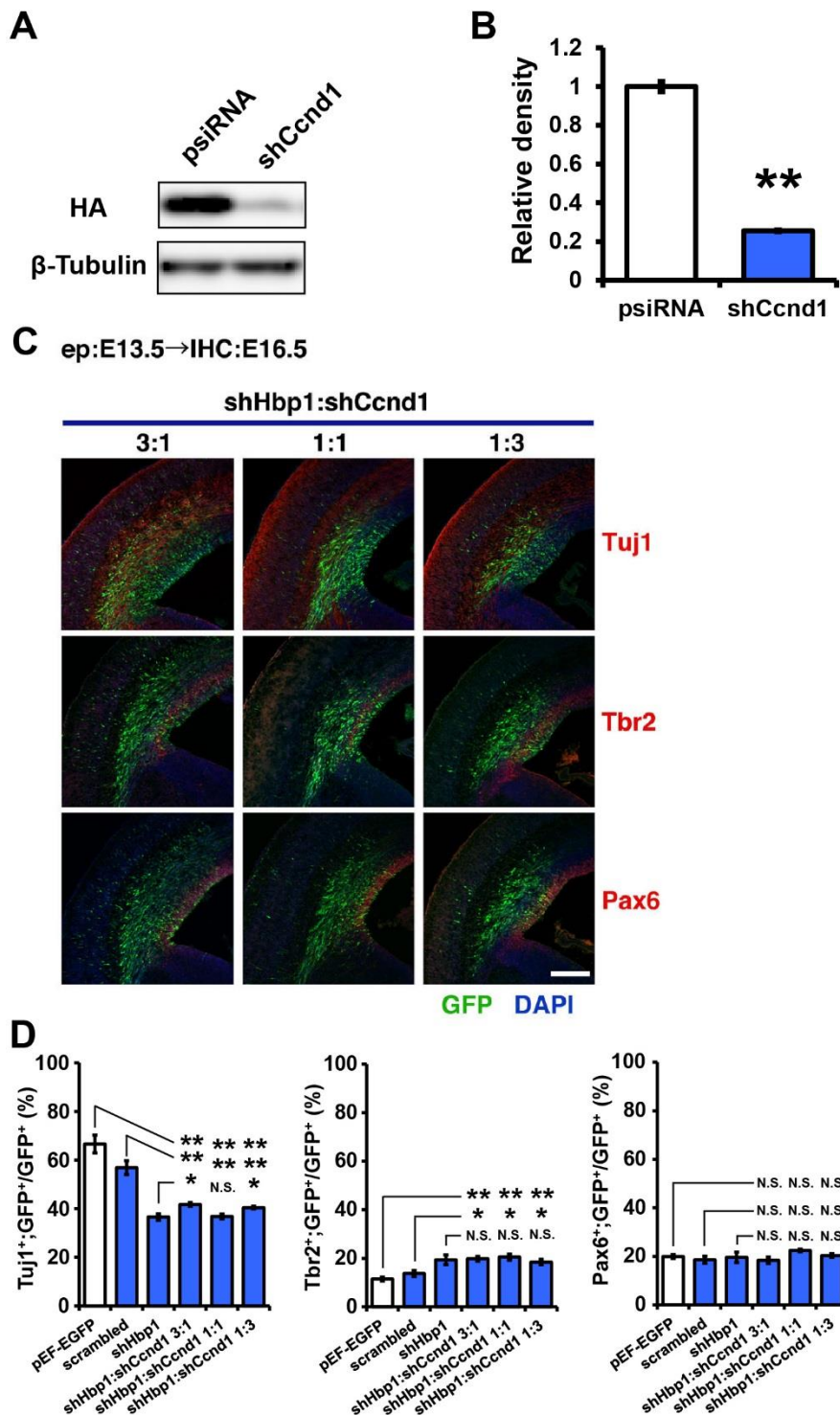**Fig. S9. Rescue experiments by knockdown of *cyclin D1*.** (**A**) Knockdown efficiency of *shCcnd1* was evaluated by western blot. HEK293T cells were co-transfected with expression vectors (*pEF-HA-Ccnd1*) that express HA-tagged cyclin D1 and expression vectors of shRNA targeting *cyclin D1* (*shCcnd1*) or negative control vectors (*psiRNA*),

and proteins were extracted from cells 24 h later. HA-cyclin D1 was detected with anti-HA antibodies. (**B**) Expression levels of HA-cyclin D1 protein were estimated as $25.58 \pm 0.01\%$ compared with the control. β-Tubulin was used as internal control, and the values were normalized to that in the control. (**C**) *shCcnd1* were co-introduced with *shHbp1* at ratios of 3:1, 1:1 or 1:3 by *in utero* electroporation at E13.5, and the fates of transfected cells were analyzed at E16.5 by immunohistochemistry using anti-GFP (green) and anti-Tuj1/Tbr2/Pax6 (red) antibodies and DAPI (blue). (**D**) Graphs showing the proportions of Tuj1^{+}, Tbr2^{+} or Pax6^{+} cells of transfected (GFP^{+}) cells 3 days after *in utero* electroporation at E16.5. *n*=3, error bars: s.e.m.; **P<0.05, **P<0.01*; Student's *t*-test; N.S., not significant. Scale bar: 200 μm.

Table S1. Primers used for PCR

Primers used for real-time PCR

Gene	Primer	Sequence
Hbp1	Fw (Forward)	5′- agttgctgcagtgtaatgagaatttg-3′
	Rv (Reverse)	5′-ggtgagtattttccggtatatctgagg-3′
Neurog2	Fw	5′-ccttcctcctggagctgcacc-3′
	Rv	5′-atacagtccctggcgaggggc-3′
Ascl1	Fw	5′-tcttagcccagaggaacaagag-3′
	Rv	5′-gcgagaaacactaaagatgcagg-3′
Neurod1	Fw	5′-ccagggttatgagatcgtcac-3′
	Rv	5′-tgagacactcatctgtccagc-3′
Cyclin D1	Fw	5′-ttgactgccgagaagttgtgc-3′
	Rv	5′-ttgttctcatccgcctctggc-3′
β-Actin	Fw	5′-ggctgtattcccctccatcg-3′
	Rv	5′-ccagttggtaacaatgccatgt-3′
		(PrimerBank ID: 6671509a1)

Primers used for preparing probes for Southern blot of genomic DNA of the ES cells

5' probe	Fw	5'-ggATCGATgatttgtaagtgatcaagtccctggc-3'
	Rv	5'-gcGTCGACgagaaggtggcttgtcaatcactacag-3'
3' probe	Fw	5'-ggATCGATtctgtaactgaattgttcacaggcca-3'
	Rv	5'-gcGTCGACtggaagcttaagatatgctgagagaag-3'

Primers used for PCR-based genotyping for *Hbp1*-floxed allele

LoxP site in intron 1	Fw	5'-tggttgggcataattttctttggtttc-3'
	Rv	5'-gcttaaacggactcatacacaaatctc-3'
LoxP-FRT site in intron 2	Fw	5'-gtccattgttatagcacttgtccagagg-3'
	Rv	5'-gcactcactctgtagaacaggttggactt-3'

Table S2. Primary antibodies

Antigen	Host	Manufacturer	Cat. No.	Dilution
<Immunohistochemistry>				
GFP	rabbit	Molecular Probes	A11122	1:200
GFP	chicken	Abcam	ab13970	1:200
Tuj1	mouse	Covance	MMS-435P	1:500
Tbr2	rabbit	Abcam	ab23345	1:500
Tbr2	rat	eBioscience	14-4875-82	1:500
Pax6	rabbit	Covance	PRB-278P	1:400
Pax6	mouse	DSHB	PAX6-s	1:100
BrdU	mouse	Molecular Probes	B35128	1:100
BrdU	rat	Serotec	MCA2060	1:500
Cux1	rabbit	Santa Cruz	sc-13024	1:100
Ctip2	rat	Abcam	ab18465	1:500
Tbr1	rabbit	Abcam	ab31940	1:100
Ki67	rabbit	Thermo	RM-9106-S0	1:100
pH3	mouse	Sigma-Aldrich	H6409-.2ML	1:200
Cyclin D1	rabbit	Thermo	RM-9104-S0	1:100
c-Jun	rabbit	Cell Signaling	#9165S	1:400
Map2	mouse	Sigma-Aldrich	M4403-100UL	1:500
p-Vimentin (Ser55)	mouse	MBL	D076-3S	1:500
Cleaved Caspase-3	rabbit	Cell Signaling	#9661S	1:500
NeuN	mouse	Merck Millipore	MAB377	1:100
Hes1	rabbit	Cell Signaling	#11988S	1:100
Olig2	mouse	EMD Millipore	MABN50	1:500
PDGFRα	rat	BD Pharmingen	558774	1:500
p-Rb (Ser780)	rabbit	Abcam	ab131264	1:200
p-Rb (Ser807/811)	rabbit	Cell Signaling	#8516S	1:500
Unc5d	goat	R&D Systems	AF1429	1:100
GFAP	mouse	Sigma-Aldrich	G3893-100UL	1:400
GABA	mouse	Sigma-Aldrich	A0310-100UL	1:500
<Western blot>				
HA conjugated to peroxidase	rat	Roche	12013819001	1:1000
p-Rb (Ser780)	rabbit	Abcam	ab131264	1:500
p-Rb (Ser807/811)	rabbit	Cell Signaling	#8516S	1:1000
β-Actin	rabbit	Sigma-Aldrich	A2066-.2ML	1:2000
β-Tubulin	rabbit	Santa Cruz	sc-9104	1:5000

Table S3. Estimation of the length of the cell cycle

The length of the cell cycle in Ki67$^+$ proliferating cells (Fig. 7D)

	E12.5		E14.5		E16.5	
	NC	icKO	NC	icKO	NC	icKO
T_C (h)	10.91 ± 0.26	8.54 ± 0.02	14.41 ± 0.12	10.47 ± 0.13	17.64 ± 0.31	13.25 ± 0.11
T_S (h)	4.72 ± 0.17	5.09 ± 0.09	5.72 ± 0.01	4.68 ± 0.16	4.12 ± 0.02	3.43 ± 0.03

The length of the cell cycle in Pax6$^+$ neural stem cells (Fig. 7E)

	E12.5		E14.5		E16.5	
	NC	icKO	NC	icKO	NC	icKO
T_C (h)	10.10 ± 0.16	6.87 ± 0.01	14.48 ± 0.06	9.30 ± 0.12	17.44 ± 0.68	12.11 ± 0.07
T_S (h)	5.70 ± 0.09	4.22 ± 0.02	5.73 ± 0.04	4.12 ± 0.01	5.72 ± 0.29	4.18 ± 0.15

The length of the cell cycle in Tbr2$^+$ neural progenitor cells (Fig. 7F)

	E12.5		E14.5		E16.5	
	NC	icKO	NC	icKO	NC	icKO
T_C (h)	21.37 ± 0.08	13.83 ± 0.25	25.38 ± 1.12	17.32 ± 0.19	27.27 ± 0.10	19.80 ± 1.27
T_S (h)	7.38 ± 0.09	5.36 ± 0.06	7.08 ± 0.15	5.04 ± 0.17	5.26 ± 0.12	3.70 ± 0.39

The length of the cell cycle in overexpression and knockdown experiments (Fig. 8F)

	T_C (h)	T_S (h)
pEF-EGFP	14.71 ± 0.38	4.73 ± 0.09
pEF-Hbp1	15.82 ± 0.10	6.01 ± 0.18
scrambled shRNA	14.64 ± 0.27	5.47 ± 0.14
shHbp1	8.54 ± 0.29	4.09 ± 0.28
shHbp1 : shCcnd1　*3:1*	11.47 ± 0.28	4.57 ± 0.39
shHbp1 : shCcnd1　*1:1*	12.10 ± 0.06	6.11 ± 0.30
shHbp1 : shCcnd1　*1:3*	13.46 ± 0.24	6.31 ± 0.16

Data are mean ± s.e.m., n = 3.